The Incomplete Transformation Phenomenon in Fe-C-Mo Alloys

W.T. REYNOLDS, Jr., F.Z. LI, C.K. SHUI, and H.I. AARONSON

The overall kinetics of isothermal transformation of austenite to bainite were studied with quantitative metallography and transmission electron microscopy (TEM) in a series of high-purity Fe-C-Mo alloys containing 0.06 to 0.27 wt pct C and 0.23 to 4.28 wt pct Mo at reaction temperatures mainly below that of the bay in the time-temperature-transformation (TTT) curve for initiation of transformation. Ferrite growth kinetics were also determined at temperatures slightly below that of the bay. The incomplete character of the bainite transformation was found to depend upon both the C and Mo concentrations; below threshold combinations of these elements, the incomplete reaction is absent. In cases in which the bainite reaction was incomplete, transformation of austenite resumed and went to completion following the initiation of Mo_2C precipitation at $\alpha:\gamma$ boundaries. The time of transformation stasis increased with the proportions of C and Mo in the alloy. Pearlite was not observed anywhere in the time-temperature-composition (TTC) region investigated. Ferrite growth kinetics at temperatures near the bay do not exhibit simple time laws; this behavior is attributed to a solute drag-like effect (SDLE). Extensive sympathetic nucleation of ferrite is observed at temperatures below that of the bay. The temperature and composition dependence of the incomplete reaction can be explained by a combination of the SDLE and the variation in the sympathetic nucleation rate of ferrite with temperature and the amount of transformation.

I. INTRODUCTION

IN the preceding paper, Shiflet and Aaronson[1] have shown that the thickening kinetics of grain boundary allotriomorphs incorporating Mo_2C carbides exhibit complex and variegated growth kinetics behavior in a number of Fe-C-Mo alloys reacted at temperatures from near that of the bay, T_b, to approximately 50 °C above this temperature. They also found no evidence for "incomplete transformation" or stasis in the bainite reaction during studies of the overall transformation kinetics performed simultaneously. During the present investigation, these studies were extended below T_b in many of these alloys. As our predecessors had found,[1] the extreme morphological degeneracy of the ferritic component of bainite below T_b severely restricted growth kinetics measurements in this temperature range. Emphasis was therefore placed upon quantitative optical metallographic studies of overall reaction kinetics, conducted for the purpose of characterizing the incomplete transformation phenomenon as a function of temperature, percent C, and percent Mo. Although such characterizations have been previously conducted on other Fe-C-X systems using physical properties measurements,[2–11] this is the first such undertaking utilizing the more reliable[12] technique of quantitative metallography. Complementary TEM studies were conducted of the ferrite and the carbide microstructures associated with critical aspects of stasis.

Inasmuch as a historical survey of the stasis phenomenon was presented as an introduction to Reference 1, summarization of background will be confined here to recent work bearing directly upon the main objectives of the present investigation. The presence of stasis in a variety of alloy steels has led to the belief that it is a general feature of the bainite reaction. In fact, it is a defining characteristic of bainite according to the widely accepted overall reaction kinetics definition.[13,14] On this view, the bainite reaction is considered to have its own "C" curve on the TTT diagram. The highest temperature of the "C" curve is designated as the kinetic bainite start, or B_s, temperature; this temperature is usually located 100 °C to 300 °C below the eutectoid temperature. The fraction of austenite which transforms to bainite increases with decreasing isothermal reaction temperature from zero at the B_s to unity at the B_f or bainite finish temperature, but bainite can form at temperatures as low as (in principle) the martensite finish temperature, M_f. The bainite reaction is thus incomplete at all temperatures between the B_s and the B_f. The absence of the incomplete reaction in some steels such as Fe-C alloys and in low-alloy steels is usually attributed to the masking of the incomplete portion of the bainite transformation by concurrent pearlite formation.[9,15–17]

An alternate view holds that incomplete transformation[14] and the shape of the TTT diagram[14,18,19] are special effects of certain alloying elements on the

W.T. REYNOLDS, Jr., formerly Graduate Student, Department of Metallurgical Engineering and Materials Science, Carnegie Mellon University, is Assistant Professor, Department of Materials Engineering, Virginia Polytechnic Institute, Blacksburg, VA 24061-0237. F.Z. LI, Visiting Professor, Department of Metallurgical Engineering and Materials Science, Carnegie Mellon University, is Professor, Department of Mechanical Engineering, Shandong Polytechnical University, Jinan, Shandong, People's Republic of China. C.K. SHUI, Visiting Professor, Department of Metallurgical Engineering and Materials Science, Carnegie Mellon University, is Professor, Department of Metallurgy and Materials Engineering, Chongqing University, Chongqing, Sichuan, People's Republic of China. H.I. AARONSON, R.F. Mehl Professor, is with the Department of Metallurgical Engineering and Materials Science, Carnegie Mellon University, Pittsburgh, PA 15213-3890.

This paper is based on a presentation made in the symposium "International Conference on Bainite" presented at the 1988 World Materials Congress in Chicago, IL, on September 26 and 27, 1988, under the auspices of the ASM INTERNATIONAL Phase Transformations Committee and the TMS Ferrous Metallurgy Committee.

precipitation of ferrite and carbides and are not general characteristics of a transformation mechanism peculiar to bainite. This view is supported by the fact that elements which induce a deep bay in the TTT diagram often produce a similar temperature dependence in the nucleation or growth kinetics of proeutectoid ferrite. Enomoto and Aaronson[20] have shown that while Mo accelerates ferrite nucleation (relative to Fe-C binary alloys) at high reaction temperatures, it reduces the nucleation rate as the reaction temperature decreases toward the bay temperature. The larger ferrite nucleation rate at high temperatures is attributed to the stabilization of ferrite by Mo; the lower nucleation rates near the bay temperature (equivalent to the B_s temperature) are caused by Mo segregation to austenite grain boundaries, which reduces the effectiveness of these sites for ferrite nucleation.[20]

The growth kinetics of ferrite and ferrite + carbide aggregates in Fe-C-Mo alloys pass through a maximum at the upper nose of the TTT diagram[21] and a minimum at the bay temperature.[1,19] They fall significantly below predicted growth kinetics at reaction temperatures below the upper nose of the TTT diagram, and the growth exponents at temperatures just above the bay often exhibit unexpected time dependencies.[1] At higher proportions of C and Mo, growth of carbide-containing grain boundary allotriomorphs is observed to cease entirely at intermediate reaction times just above the bay temperature.[1] Growth of the allotriomorphs resumes after a period termed "growth stasis."[1] In addition, ferrite formed below the bay temperature in Fe-C-Mo and Fe-C-Cr alloys often has an unusually degenerate Widmanstätten morphology.[19] This collection of effects upon growth has been interpreted as evidence for a proposed SDLE of Mo upon ferrite growth.[21,22] Taken together, the special effects of Mo on the nucleation and growth of ferrite suggest that the key features associated with the overall reaction kinetics definition of bainite (the separate C-curve and the incomplete transformation phenomenon) may actually be characteristic of specific alloying elements and not of the fundamental transformation mechanism itself.

This investigation was initiated to determine the relative merits of the overall reaction kinetics and the "special element" views of bainite by testing the generality of the incomplete transformation phenomenon, a key feature of the former view, in a number of selected high-purity Fe-C-Mo alloys. This system was selected for investigation primarily because Mo induces a deep bay in the TTT diagram. This trait facilitates study of the kinetic features of bainite. Additionally, the pearlite reaction is severely restricted in Fe-C-Mo alloys[1,23–25] and does not interfere with bainite formation below T_b. High-purity alloys were used to avoid the complication of interactive effects among multiple solutes. A companion paper extends this investigation to Fe-C-Si, Fe-C-Mn, Fe-C-Ni, and Fe-C-Cu alloys.[26] An effort was also made to augment data from a predecessor investigation on the growth kinetics of ferrite allotriomorphs in Fe-C-Mo alloys reacted at temperatures above T_b.[1] Since the relief exhibited by bainite when formed at a free surface has often been used to infer the mechanism of the bainite reaction,[27,28,29] the nature of the surface relief produced by bainite in a representative Fe-C-Mo alloy was also investigated.

II. EXPERIMENTAL PROCEDURE

The alloys employed (Table I) were prepared by vacuum induction melting. The C concentrations ranged from 0.064 to 0.24 wt pct, and the Mo concentrations were between 0.23 and 4.28 wt pct. Ingots were redundantly hot worked and then homogenized at either 1250 °C or 1300 °C for 3 days in purified Ar. Chemical analysis was performed on each alloy before and after homogenization to assure that no change in the C concentration occurred during this procedure. Coupons 10 × 10 × 0.5 mm in size were austenitized at 1300 °C for 900 seconds in a deoxidized salt bath[30] and isothermally reacted in deoxidized Pb before quenching in iced brine. The progress of the overall transformation was measured by point counting[31,32] specimens isothermally reacted for successively longer times. The metallographic procedure is described in detail in Reference 33.

Specimens from representative alloys, reacted for selected transformation times and temperatures, were examined with TEM to ascertain the type, morphology, and distribution of the carbides present at various stages of transformation as well as to elucidate some details of the ferrite microstructures. Thin foil specimens were prepared by jet polishing in a 30 pct HNO_3, 70 pct methanol solution at −50 °C and 10 to 20 V. Observations were carried out in a JEM 120CX operated at 120 kV.

Growth kinetics of grain boundary ferrite allotriomorphs were measured in thin specimens (10 × 10 × 0.25 mm) according to the method employed by Bradley

Table I. Fe-C-Mo Alloy Compositions

Wt Pct C	At. Pct C	Wt Pct Mo	At. Pct Mo	Wt Pct Mn	Wt Pct Si	Wt Pct P	Wt Pct S
0.22	1.02	0.23	0.13	<0.003	0.03	0.002	0.003
0.13	0.60	0.46	0.27	<0.003	0.03	0.003	0.003
0.09	0.40	0.94	0.55	<0.003	0.03	0.002	0.003
0.15	0.70	0.92	0.53	<0.003	0.03	0.002	0.003
0.24	1.11	0.93	0.54	<0.003	0.03	0.002	0.003
0.06	0.30	1.80	1.05	<0.002	0.002	0.005	0.002
0.19	0.88	1.81	1.06	<0.002	0.004	0.006	0.002
0.26	1.21	2.31	1.34	<0.002	0.02	0.006	0.002
0.27	1.26	3.19	1.86	<0.002	0.004	0.005	0.003
0.26	1.22	4.28	2.51	<0.002	0.02	0.005	0.004

et al.[34] but with several notable differences. Grain growth during austenitization at 1300 °C was not rapid enough in the alloys used to allow austenite grains to grow entirely through the thin dimension of the specimens. The specimen thickness generally contained two austenite grains which met along the center plane of the specimen. The austenite grain boundaries were approximately perpendicular to the specimen surfaces, except near the specimen center. To avoid stereological errors in the growth kinetics measurements, the plane of polish was located about midway between the surface and the center plane of each specimen. Also, grain boundary ferrite allotriomorphs in these alloys almost always grew into only one of the two bounding austenite grains at the reaction temperatures employed. Accordingly, the thickness rather than the half-thickness of the allotriomorphs is reported here as a function of isothermal reaction time.

For the surface relief investigation, the technique originally employed by Ko and Cottrell was used.[27] Polished specimens of the Fe-0.19 wt pct C-1.81 wt pct Mo alloy (10 × 5 × 0.5 mm) were encapsulated in quartz under 0.34×10^5 Pa (1/3 atm) of purified He, austenitized at 1300 °C for 900 seconds, quenched in Pb at 585 °C and reacted for 600 seconds, and then up-quenched to 750 °C for 1000 seconds to further transform the austenite. Transformation at 750 °C helped to separate surface relief effects resulting from transformation at 585 °C from those due to martensite formed during the final quench from 750 °C to room temperature. The capsules were not broken until after they had reached room temperature. The surfaces of the transformed specimens were then examined using optical interference microscopy to determine the nature of the surface reliefs produced by the transformation products.

III. RESULTS

A. *Morphology of Bainite*

Many features of the isothermal transformation of austenite are common to all of the Fe-C-Mo alloys studied. To avoid repetition, the results obtained on a representative alloy, Fe-0.19 wt pct C-1.81 wt pct Mo, will be presented, and the effect of changing the Mo and C concentration will then be discussed relative to these prototypical results. The TTT diagram for the Fe-0.19 wt pct C-1.81 wt pct Mo alloy is shown in Figure 1. As usual in these alloys, there are two temperature regions in which transformation begins relatively quickly. These two regimes are separated by a bay in the TTT diagram. The temperature at which the transformation initiation time is a maximum is designated as the bay temperature, or T_b. This temperature corresponds to the kinetically defined bainite start temperature.[14] Transformation above the bay begins at austenite grain boundaries (Figure 2(a)).[1,19,24] Above the upper nose, ferrite nucleates first and is followed soon after by the initiation of alloy carbide precipitation.[23] M_6C carbides form allotriomorphically on austenite grain boundaries and at ferrite:austenite boundaries; Mo_2C carbides precipitate at ferrite:austenite boundaries as fibers or as interphase boundary carbides and as Widmanstätten rods within ferrite.[1,23,24,35] Below the upper nose and above T_b, ferrite and carbides precipitate concurrently from practically the

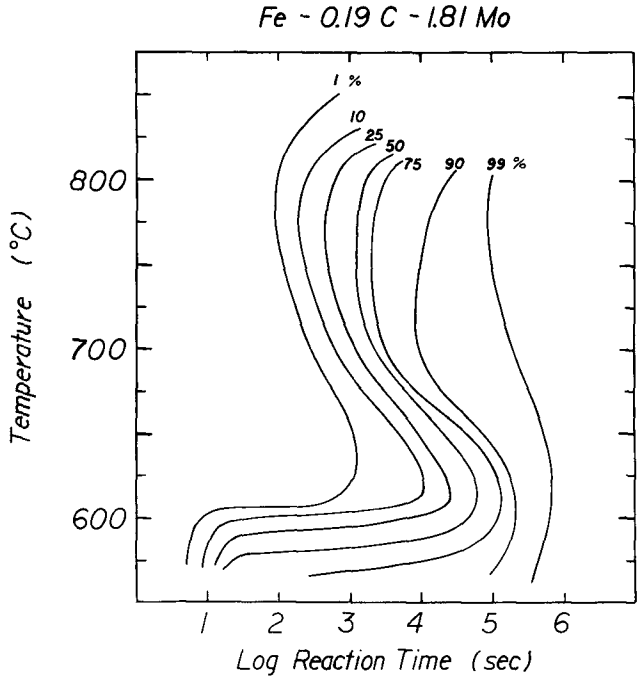

Fig. 1—The TTT diagram for Fe-0.19 wt pct C-1.81 wt pct Mo; the bay temperature is approximately 615 °C.

earliest stage of transformation.[23] Unlike most plain C steels, Widmanstätten ferrite is increasingly absent at reaction temperatures between the upper nose and T_b[19,24] in alloys containing more than approximately 1.0 wt pct Mo. Grain boundary allotriomorphs become the sole ferrite morphology at and just above the bay temperature[1] with increasing Mo and C concentrations.

At isothermal reaction temperatures below T_b, ferrite assumes a highly degenerate Widmanstätten morphology (Figure 2(b)).[19,24] The transition from the allotriomorphic morphology at temperatures above T_b to degenerate, grain boundary-nucleated ferrite is quite sharp with decreasing reaction temperature, occurring within a temperature interval of about 10 °C. Some allotriomorphic ferrite is still present a few tens of degrees Celsius below T_b, but the largest proportion of ferrite consists of the degenerate morphology. At slightly lower temperatures, allotriomorphs are almost entirely absent.

At the beginning of transformation, the distribution of degenerate ferrite is nonuniform. Some austenite grains are highly transformed, while others contain little or no degenerate ferrite. The degenerate structure initially consists of proeutectoid ferrite; carbides are not present (Figure 2(d)). Transmission electron microscopy examination reveals that the ferrite is composed of irregularly shaped crystals 0.5 to 3 μm on a side. These crystals are essentially the same as the "substructural units" or "subunits" reported by Oblak and Hehemann in a variety of steels.[36] They appear equiaxed in alloys containing greater than approximately 2 wt pct Mo. In more dilute alloys (Figure 2(c)), the ferrite is angular in appearance and is similar to more classical forms of degeneracy[37] (*cf.* Figures 2(b) and (c)).

The subunits form by sympathetic nucleation,[36,38] *i.e.*, by the nucleation of new ferrite crystals at the ferrite:austenite boundaries of existing ferrite crystals.[39,40] It has been suggested that these subunits grow by a rapid,

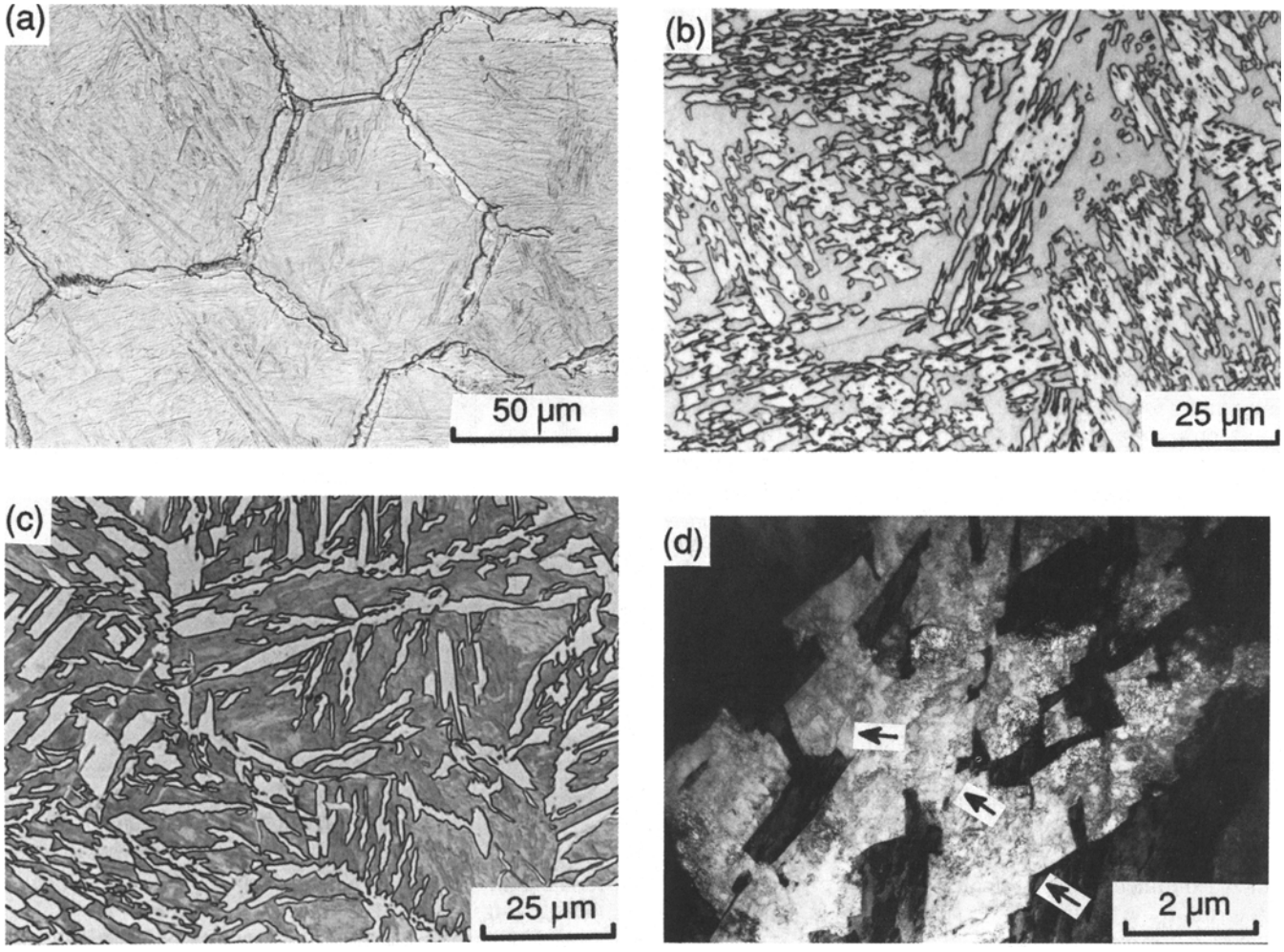

Fig. 2—Ferrite and bainite morphologies: (*a*) allotriomorphic ferrite + carbide, Fe-0.19 wt pct C-1.81 wt pct Mo reacted at 625 °C for 10,000 s (10 °C above T_b); (*b*) degenerate ferrite, Fe-0.19 wt pct C-1.81 wt pct Mo reacted at 585 °C for 300 s (30 °C below T_b); (*c*) degenerate ferrite, Fe-0.2 wt pct C-0.93 wt pct Mo reacted at 630 °C for 49 s (20 °C below T_b); and (*d*) degenerate ferrite formed by sympathetic nucleation, Fe-0.19 wt pct C-1.81 wt pct Mo reacted at 585 °C for 600 s.

self-accommodating shear mechanism.[36] However, thermionic emission measurements of lengthening and thickening kinetics of individual subunits demonstrate that they form much more slowly, probably by the diffusion-controlled migration of growth ledges.[41] The degenerate, or ragged, appearance of ferrite formed at temperatures below T_b apparently results from the misalignment of adjacent ferrite crystals. Evolution of precipitate plates by the successive sympathetic nucleation of small crystals has also been observed during other diffusional transformations, such as the precipitation of the hcp α phase from bcc β in Ti-Cr[40] and in the formation of cementite plates from austenite in a hypereutectoid Fe-C-Mn alloy.[42] However, the microstructures produced in the latter transformations are much more symmetrical and uniform. An exceptionally high rate of nucleation of new ledges at α:α boundaries formed by sympathetic nucleation may be partially responsible for this difference.

B. *Ferrite + Carbide Mixtures*

In agreement with previous observations,[1,19,21,23] lamellar pearlite is entirely absent at temperatures near the bay in Fe-C-Mo alloys. Because fibrous Mo_2C carbides grow cooperatively with ferrite at temperatures above T_b,[1,23] they can be considered to be an alloy carbide, rod-type of pearlite.[43] However, the fibrous reaction occurs in conjunction with the interphase boundary mode of carbide precipitation,[1,23] so the upper "C" curve of the TTT diagram cannot be ascribed uniquely to a pearlitic reaction mechanism, classical views to the contrary.

During the final stages of transformation at temperatures from the upper nose down to slightly below the bay, nodular bainite, a coarse mixture of cementite and ferrite, forms in alloys containing more than about 0.1 wt pct C and 0.5 wt pct Mo (Figure 3).[25] This constituent usually comprises less than 5 pct of the total microstructure but can constitute up to 17 pct of it in some of the Fe-C-Mo alloys studied.[25]

C. *Surface Relief Effects*

The carbide-free, degenerate ferrite morphology does not produce a clear surface relief or tilt. The optical and interference micrographs in Figure 4 show a free surface of the Fe-0.19 wt pct C-1.81 wt pct Mo alloy following the 1300 °C to 585 °C to 750 °C step quenching

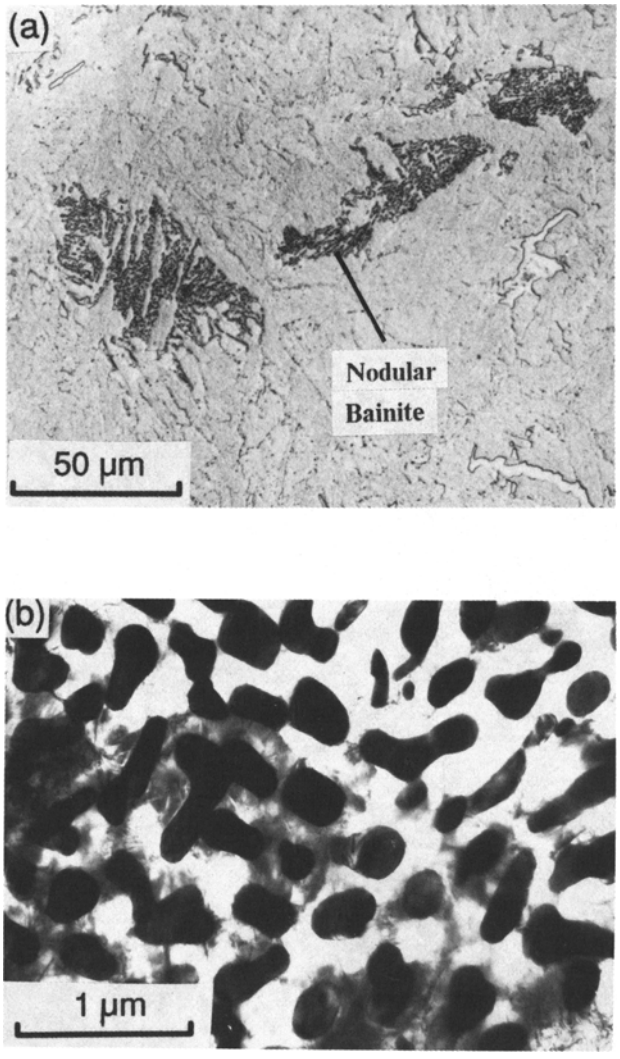

Fig. 3—Nodular bainite composed of ferrite and cementite, Fe-0.24 wt pct C-0.93 wt pct Mo: (*a*) optical, 640 °C, 258,700 s and (*b*) TEM, 660 °C, 18,300 s.

experiment. An example of a region of degenerate ferrite and the surface rumpling type of relief usually associated with this morphology is indicated at "DF." The prominent linear reliefs in some regions of Figure 4 are formed during the continuation of transformation at 750 °C. Hence, neither the invariant plane strain reliefs associated with both martensitic and diffusional growth of plate-shaped transformation products nor the tent-shape reliefs which are often produced during the latter type of transformation are found in conjunction with the degenerate ferrite comprising the predominant transformation product below T_b.

D. *Overall Reaction Kinetics*

At temperatures above the bay, isothermal transformation curves (fraction of austenite transformed *vs* the logarithm of the reaction time) display a characteristic sigmoidal shape (Figure 5(a)). After a relatively slow initiation period, the amount of transformation increases smoothly to approximately 100 pct. This behavior was well documented during investigations in a variety of steels in the 1930's,[2,6,8] as well as more recently in many Fe-C-Mo alloys.[1]

Transformation below the bay occurs in up to three distinct stages, as typified by Figure 5(b). The first stage takes place with rapid kinetics.[2,6,8] Although transformation is presumably initiated by nucleation and growth at the austenite grain boundaries, sympathetic nucleation appears to provide the source of a large majority of the ferrite crystals formed during this initial stage of transformation. In agreement with earlier observations,[36] the individual ferrite crystals appear to cease growing after reaching a size of a few microns. The micrograph in Figure 2(d) is a typical first-stage microstructure.

The beginning of the second stage of transformation is identified by an abrupt decrease in the transformation rate (Figure 5(b)). This is associated with cessation of the sympathetic nucleation of ferrite. Transformation is sluggish during this stage and, under some conditions, stops entirely (*e.g.*, Figures 13(g) and (h)). Cessation of transformation will be referred to here as "transformation stasis" and is the same as incomplete transformation, as defined by Griffiths *et al.*[15]* Although carbides were not detected with TEM either prior to or during the stasis period (Figure 6(a)), very small carbides, approximately 1 nm in diameter, were found at boundaries between ferrite crystals during stasis using a field ion microscope/atom probe (FIM/AP).[44]

*Transformation stasis requires that both nucleation and growth of the product phase stop. This is distinct from growth stasis[1] during which only growth ceases.

The third stage of transformation commences when the transformation curve becomes steeper (Figure 5(b)) and continues until the transformation of austenite is completed (>99 pct transformed). The acceleration of transformation is associated with the beginning of Mo_2C precipitation by the interphase boundary precipitation mechanism (Figure 6(b)). Figure 6(c)), a carbide dark-field image of a portion of the ferrite:austenite interface in Figure 6(b), shows the carbides on the terraces of ferrite ledges; they appear as rows in this edge-on view. The faint, nearly horizontal boundary which crosses the micrograph in Figure 6(b) (indicated by arrows) is the location where interphase boundary precipitation began. Below this line, a few isolated carbides have precipitated on dislocations within the ferrite. Above the line, the density of Mo_2C is much higher due to the formation of the interphase boundary carbides. Since interphase boundary carbides are only observed during the third stage of transformation, the ferrite in the lower portion of Figure 6(b) probably formed during the first stage (before transformation stasis). Transformation thus resumes following stasis with the precipitation of Mo_2C at ferrite:austenite interfaces.

The fraction transformed at the beginning of the second stage decreases as the reaction temperature is increased and eventually goes to zero at T_b, in accord with the long-established behavior of the incomplete transformation phenomenon.[13] For the Fe-0.19 wt pct C-1.81 wt pct Mo alloy shown in Figure 5, transformation stasis is present at 600 °C and 585 °C (Figures 13(g) and (h)). Transformation stasis is observed to disappear with decreasing reaction temperature before the stasis plateau

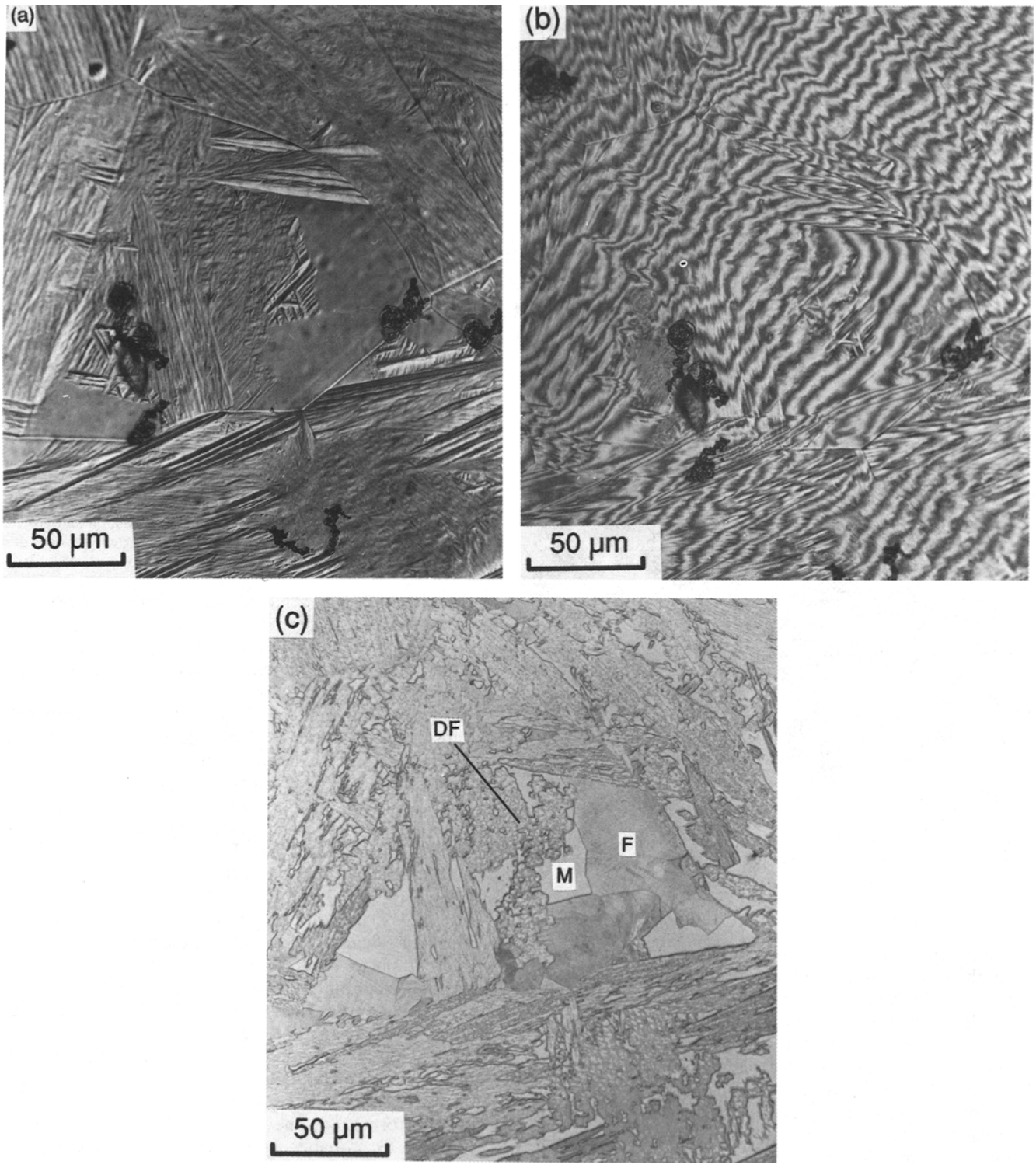

Fig. 4—Surface relief exhibited by the Fe-0.19 wt pct C-1.81 wt pct Mo alloy, reacted at 585 °C for 600 s, up-quenched to 750 °C for 1000 s, then quenched into iced brine, (*a*) Nomarski interference contrast micrograph of the as-reacted surface; (*b*) interference contrast, same region as shown in (a); and (*c*) same region as shown in (a) and (b) after light polishing and etching; F = grain boundary ferrite, DF = degenerate ferrite; and M = martensite.

reaches a level of 100 pct transformation. For example, at 570 °C (Figure 13(i)), the second stage begins after 70 pct of the austenite has transformed, but *there is no transformation stasis at this temperature*; the transformation rate during the second stage remains finite. Consequently, a bainite finish temperature, as presently defined,[13] does not appear to exist in these alloys.

The presence of transformation stasis at temperatures below T_b is dependent on both the C and the Mo concentrations in the alloy. Figures 7 through 16 show

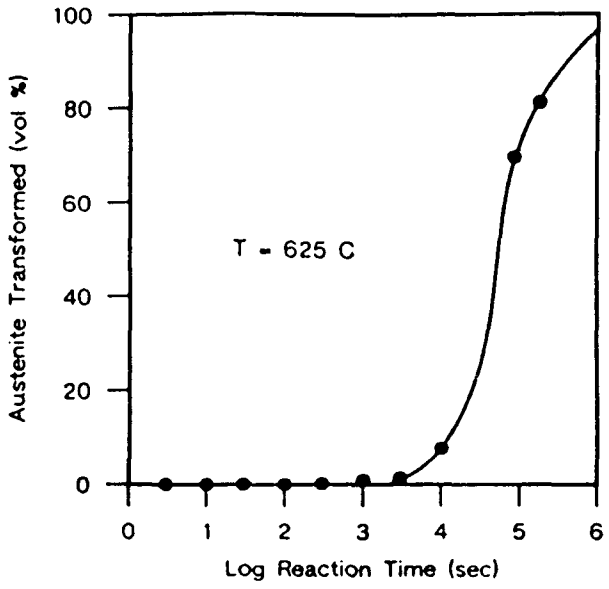

(*a*)

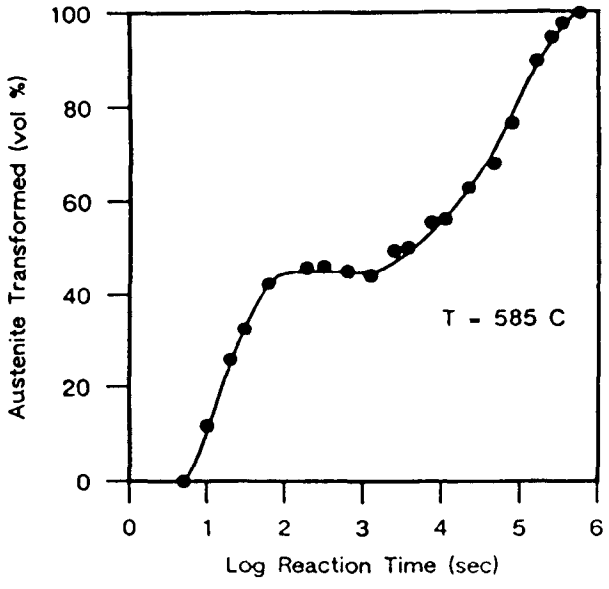

(*b*)

Fig. 5—Isothermal transformation curves for Fe-0.19 wt pct C-1.81 wt pct Mo; the bay temperature for this alloy is 615 °C: transformed at (*a*) 625 °C and (*b*) 585 °C.

the transformation kinetics for all of the Fe-C-Mo alloys studied. In general, increasing the Mo or C concentration in the alloy accentuates the three stages of transformation and encourages the development of transformation stasis below T_b. Increasing the Mo content of an approximately constant C level greatly extends the duration of the second and third stages of transformation (Figures 7, 11, and 14 through 16). *Below minimum threshold combinations of C and Mo concentrations, transformation stasis is not observed.* This result is summarized in Figure 17, which shows the alloy compositions in which transformation stasis is and is not found at temperatures below T_b. The boundary in Figure 17 separates the transformation stasis and no-stasis regimes. In alloy compositions approaching the no-stasis boundary from the stasis side, the duration of the stasis period becomes shorter. Once the boundary is crossed, the transformation rate during the second stage of transformation becomes nonzero and increases slowly with decreasing C or Mo concentration (Figures 11 and 8). When either of these concentrations is sufficiently diminished, it seems likely that the second stage will smoothly disappear within a single sigmoidal transformation curve, though such behavior has yet to be experimentally established. In effect, though, the existence of another boundary, between one- and three-stage overall transformation kinetics, seems inevitable.

E. *Thickening Kinetics of Grain Boundary Ferrite Allotriomorphs*

The thickening kinetics of grain boundary ferrite allotriomorphs at temperatures below T_b are difficult to secure in Fe-C-Mo alloys due to the degeneracy of the ferrite morphology,[19,24] particularly in higher Mo alloys and at large undercoolings below T_b. As a consequence, the lowest Mo alloy in our set of steels (Table I) which exhibits transformation stasis, Fe-0.24 wt pct C-0.93 wt pct Mo, was employed to measure the thickening kinetics of ferrite allotriomorphs in an attempt to make a connection between transformation stasis and growth kinetics. Ferrite growth kinetics at and slightly below the bay temperature are presented in Figure 18 as graphs of the log of allotriomorph thickness *vs* the log of the reaction time. At 650 °C (the bay temperature for this alloy) and 640 °C, the growth kinetics exhibit two stages. The first stage has a smaller slope than the second. The transition between the stages occurs at approximately 50 seconds at 650 °C and at approximately 80 seconds at 640 °C. There are also two growth stages at 630 °C, but the first stage has faster kinetics than the second. The transition from first- to second-stage growth occurs at about 15 seconds at this temperature.

The growth kinetics can be described by a power law: $S = \alpha t^n$, where S is the distance the ferrite:austenite interface has grown in time t, n is the time exponent, and α is a proportionality constant. For diffusion-controlled growth of a planar, disordered ferrite:austenite boundary, $n = 0.5$, and α becomes the parabolic rate constant.[45,46] Table II contains the values of α and n determined by a least-squares analysis for stage-one and state-two growth at 650 °C, 640 °C, and 630 °C. The time exponent for stage 1 growth was 0.28 at 650 °C and 0.18 at 640 °C, both significantly less than the value of 0.5 expected during conventional volume diffusion-controlled growth. The corresponding exponent at 630 °C was 0.46.

The time exponent during the second growth stage increased to 0.48 and 0.51 at 650 °C and 640 °C, respectively. At 630 °C, the exponent decreased from 0.46 during stage 1 to 0.27 during stage 2. The measured rate constants, α, during the second growth stage at 650 °C and 640 °C (the stage 2 kinetics at these temperatures are approximately parabolic) were 1.14 and 0.78 $\mu m/s^{1/2}$. Calculated values of α are also included in Table II for comparison. Following Bradley and Aaronson,[47] the growth constants for the thickening of

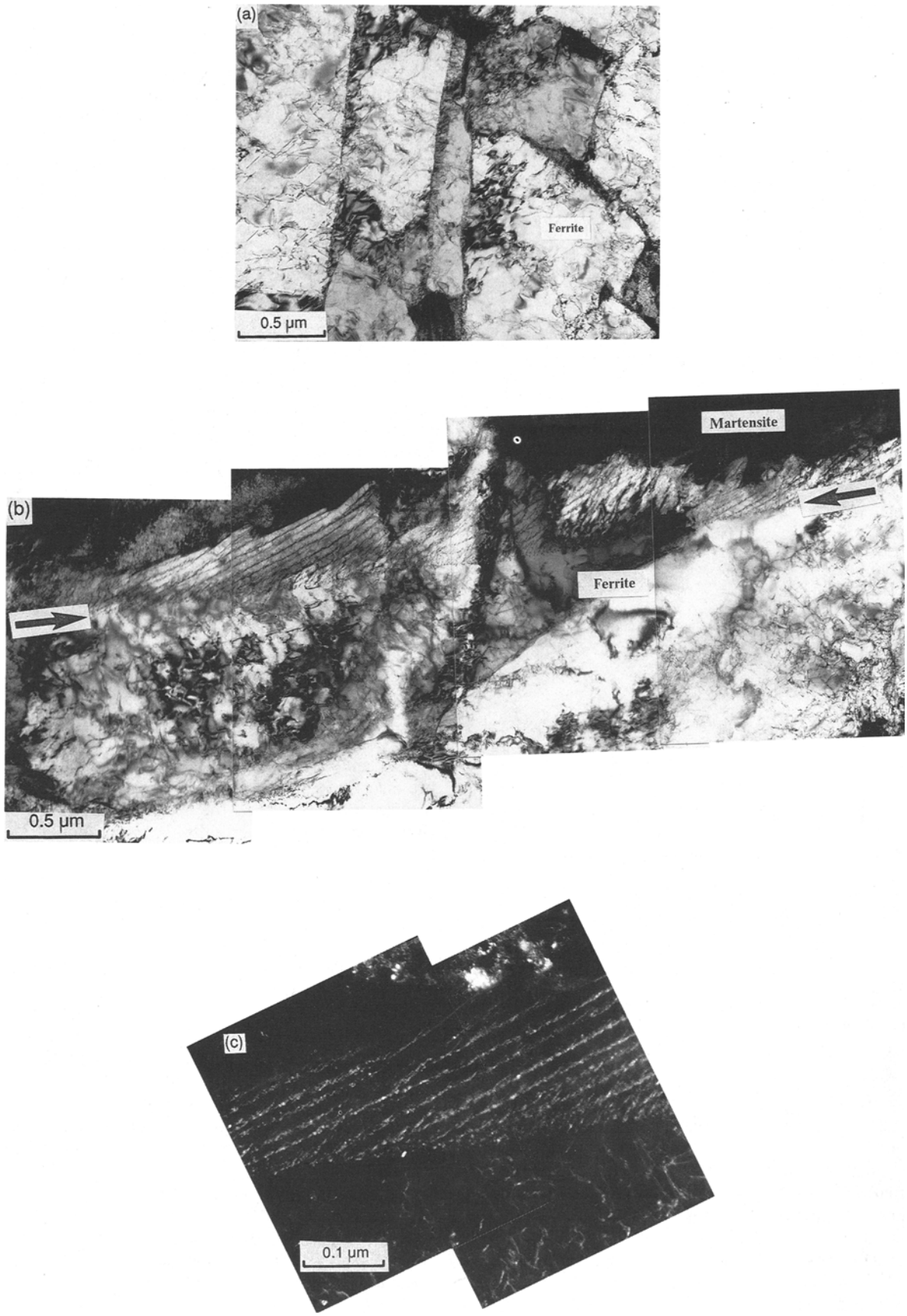

Fig. 6—TEM microstructure of Fe-0.19 wt pct C-1.81 wt pct Mo transformed at 585 °C: (*a*) reacted for 600 s (stage 2, transformation stasis) (note sympathetically nucleated ferrite crystals and no visible carbides); (*b*) reacted for 21,600 s (stage 3), illustrating interphase boundary carbide precipitation (the initiation of stage 3 growth is indicated by arrows); and (*c*) dark-field micrograph of interphase boundary carbides shown in (b).

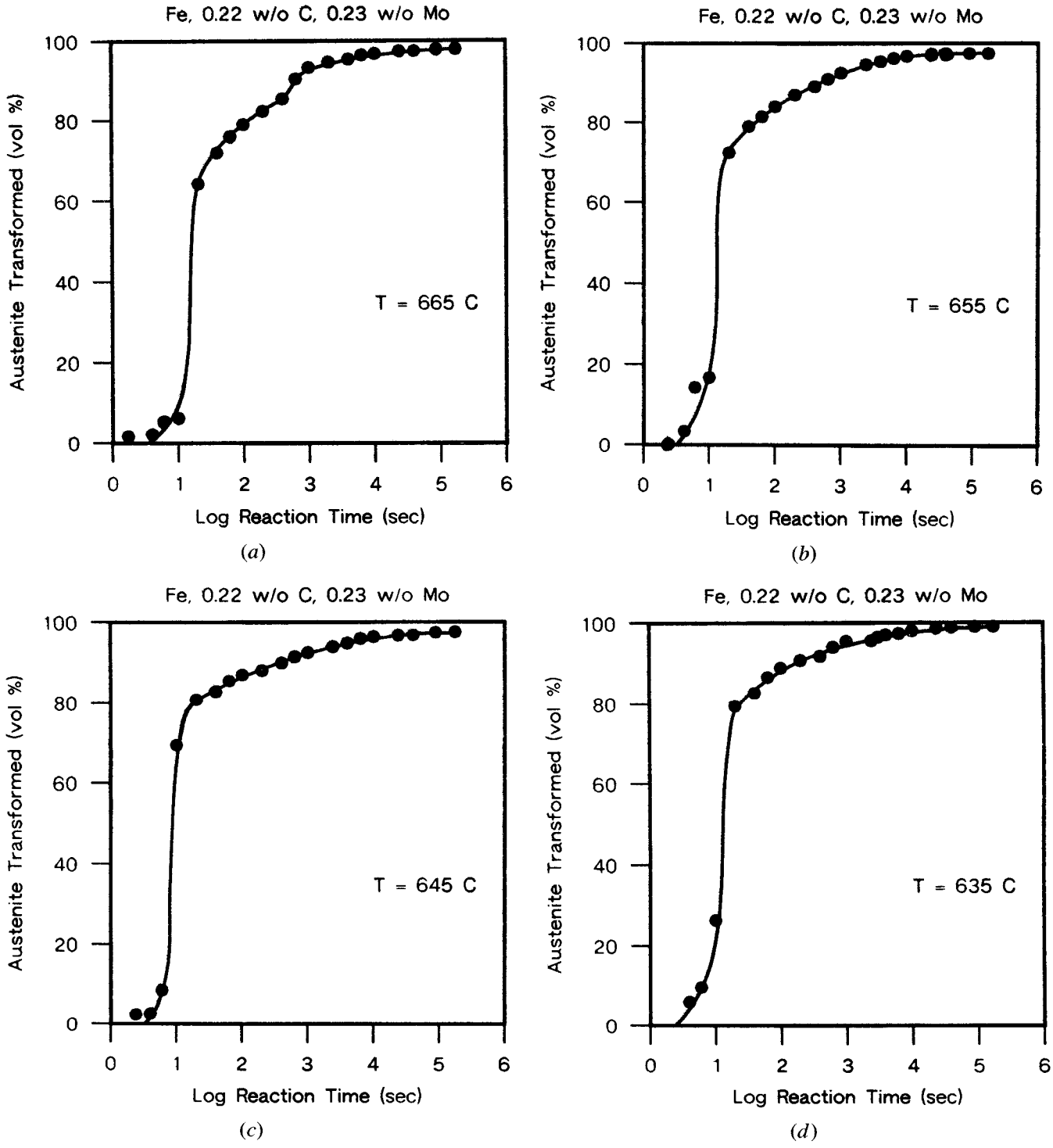

Fig. 7—Isothermal transformation curves for Fe-0.22 wt pct C-0.23 wt pct Mo; the bay temperature is 685 °C transformed at (*a*) 665 °C, (*b*) 655 °C, (*c*) 645 °C, and (*d*) 635 °C.

ferrite allotriomorphs were calculated assuming a disordered, planar interface. The carbon concentrations in ferrite and in austenite at the advancing interphase boundary were obtained from the paraequilibrium[48,49] phase diagram* determined using the thermodynamic model of Hillert and Staffansson[50] and the tabulated thermodynamic parameters of Uhrenius.[51] The concentration dependence of the carbon diffusivity in austenite was incorporated in the analysis by employing a weighted average[52] of the composition-dependent carbon diffusivity given by Kaufman *et al.*[53] The calculated paraequilibrium rate constants at 650 °C and 640 °C were 2.13 and 2.10 $\mu m/s^{1/2}$, respectively; these are approximately twice the measured values during the second, or most nearly parabolic, stage of growth.

*Paraequilibrium is a constrained equilibrium in which only carbon atoms are free to partition between ferrite and austenite. The ratio of the substitutional solute concentration to the iron concentration is the same in ferrite and in austenite; the chemical potential of carbon is equal in the two phases.[49]

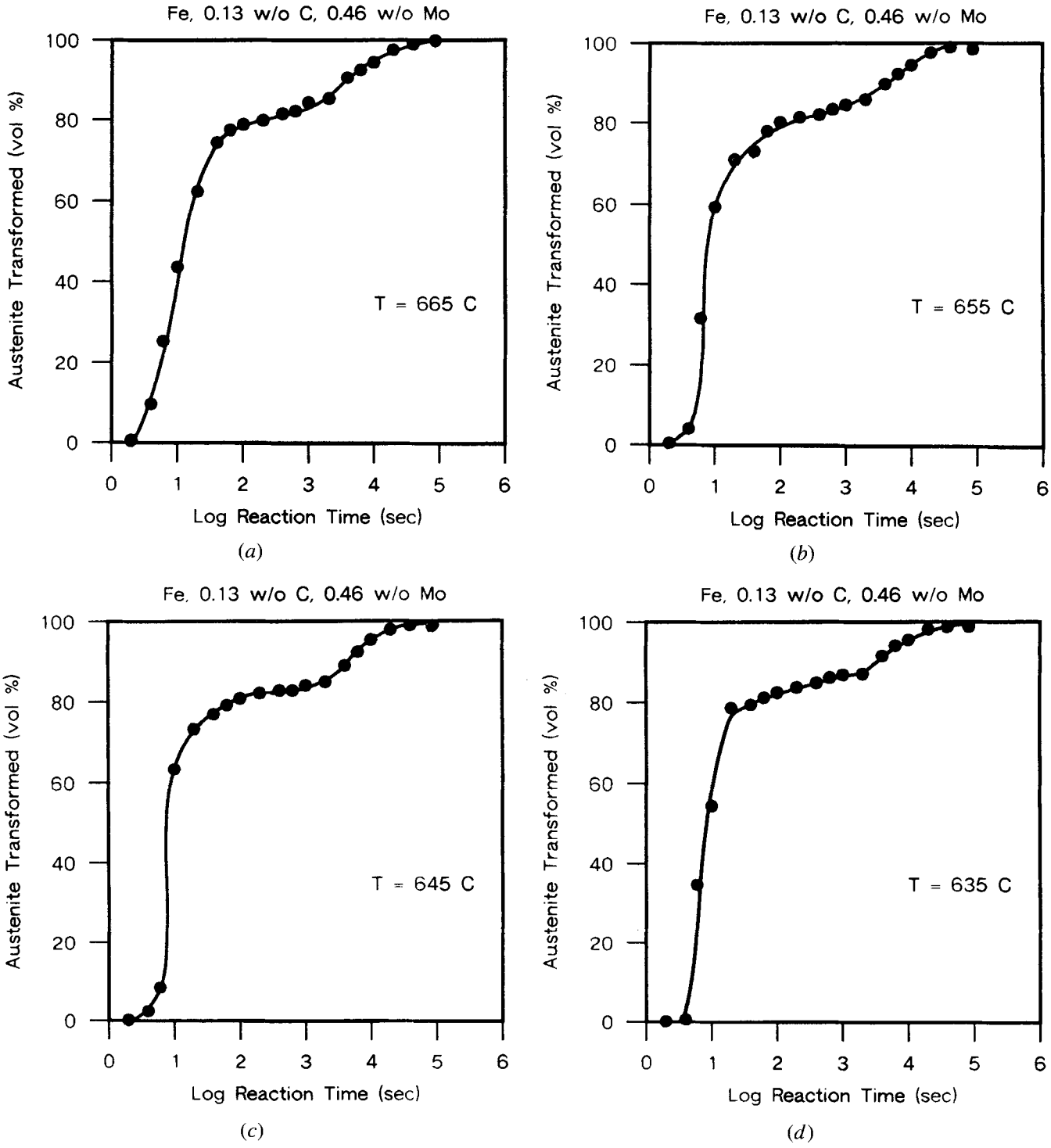

Fig. 8—Isothermal transformation curves for Fe-0.13 wt pct C-0.46 wt pct Mo; the bay temperature is 675 °C: transformed at (*a*) 665 °C, (*b*) 655 °C, (*c*) 645 °C, and (*d*) 635 °C.

IV. DISCUSSION

Numerous explanations for the incomplete transformation phenomenon have evolved since its discovery. The earliest one, due to Wever and Mathieu[4] and Wiester,[5] maintains that the incomplete nature of the bainite reaction results from strain energy accumulation associated with the precipitation of bainite from austenite. The strain energy increases with the volume fraction of the transformation product until the free energy change accompanying the transformation is no longer large enough to support the reaction. This view is analogous to a standard explanation for the athermal nature of martensite formation in steel.[54] However, this explanation contains a number of flaws. Much of the strain associated with bainite (or ferrite) precipitation should be relieved by plastic deformation, particularly in the temperature range associated with incomplete transformation. It is also unclear why transformation strain

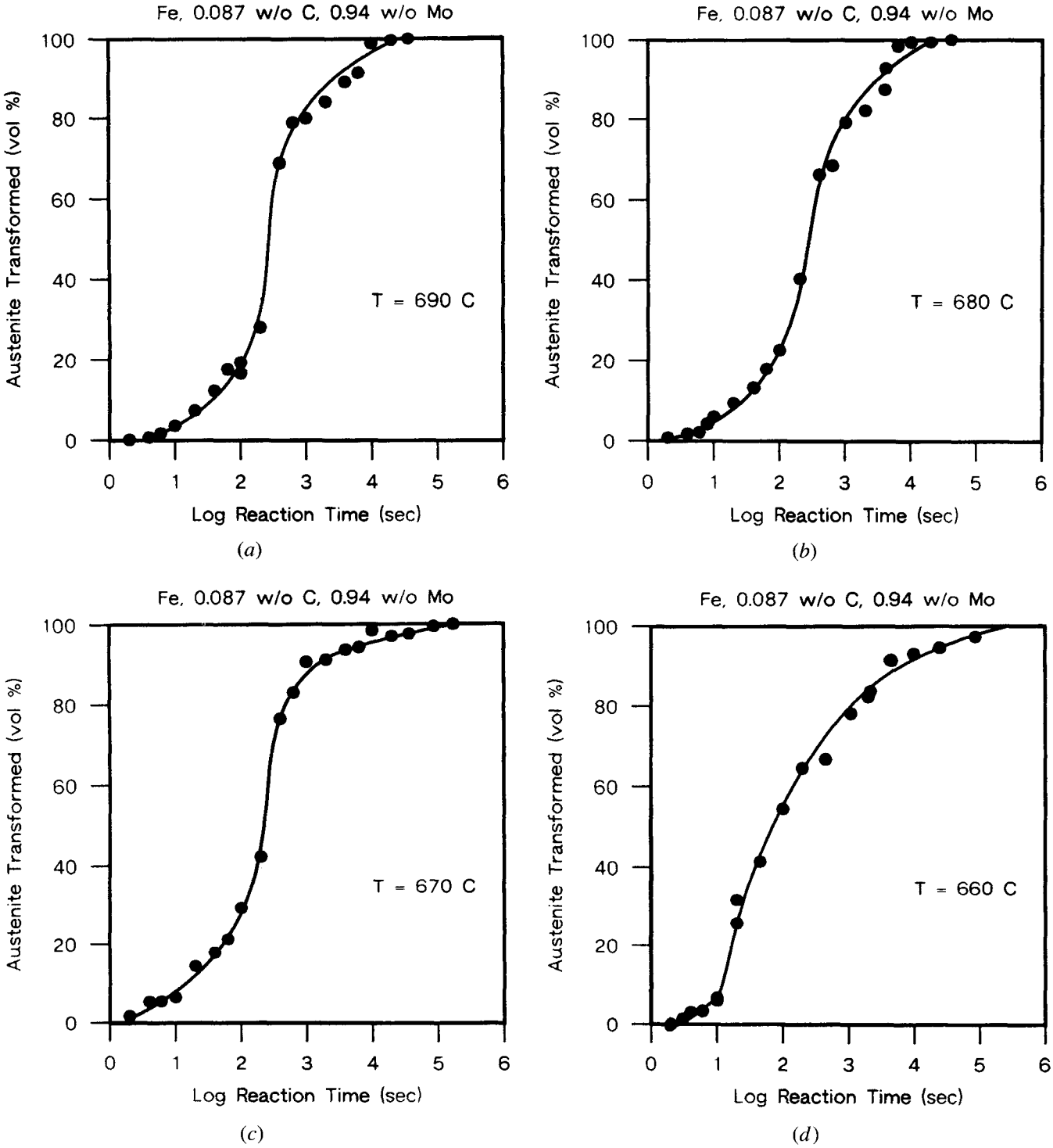

Fig. 9—Isothermal transformation curves for Fe-0.087 wt pct C-0.94 wt pct Mo; the bay temperature is 670 °C: transformed at (*a*) 690 °C, (*b*) 680 °C, (*c*) 670 °C, (*d*) 660 °C, (*e*) 650 °C, (*f*) 640 °C, and (*g*) 630 °C.

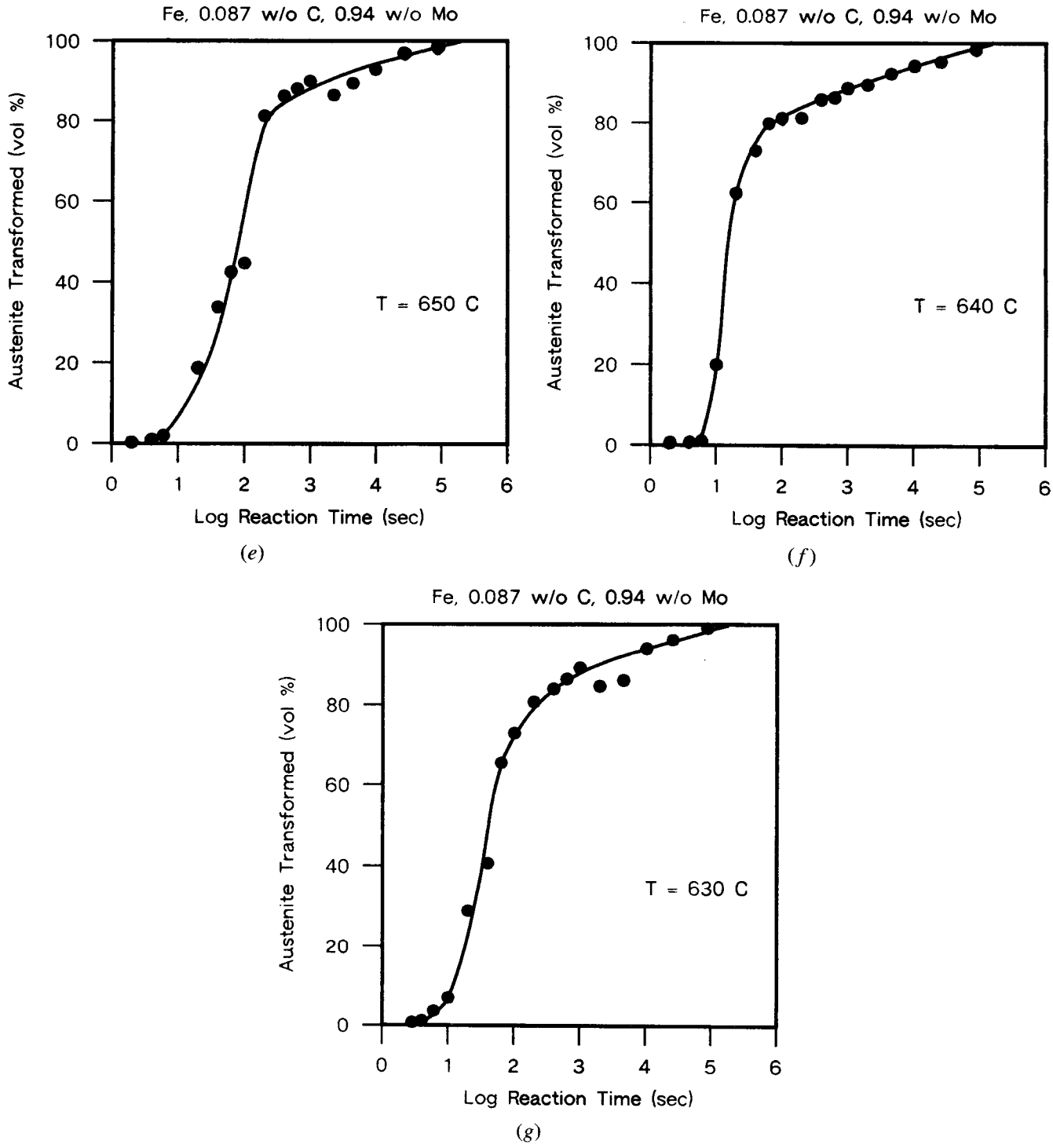

Fig. 9 Cont.—Isothermal transformation curves for Fe-0.087 wt pct C-0.94 wt pct Mo; the bay temperature is 670 °C: transformed at (*a*) 690 °C, (*b*) 680 °C, (*c*) 670 °C, (*d*) 660 °C, (*e*) 650 °C, (*f*) 640 °C, and (*g*) 630 °C.

energy does not affect proeutectoid ferrite precipitation in the same way as it affects bainite formation. The Widmanstätten ferrite start temperature does not generally coincide with the B_s temperature (*i.e.*, T_b in the present context) in Fe-C-X alloys,[14] and Widmanstätten ferrite does not exhibit the incomplete transformation phenomenon. Furthermore, the strain energy explanation does not account for the sensitive composition dependence of transformation stasis. While the presence of stasis depends upon the nature of the X element[26] and, in Fe-C-Mo alloys, upon the concentrations of C and of Mo as well, the transformation strain energy should be relatively insensitive to these factors in dilute Fe-C-X alloys.

Wiester[5] and Klier and Lyman[10] postulated that carbon atoms spontaneously rearrange in austenite at the isothermal reaction temperature; the low-carbon regions then transform to bainite by a martensitic mechanism. The extent of transformation depends on the volume of the low-carbon regions. The proposed carbon rearrangement is essentially equivalent to spinodal decomposition.

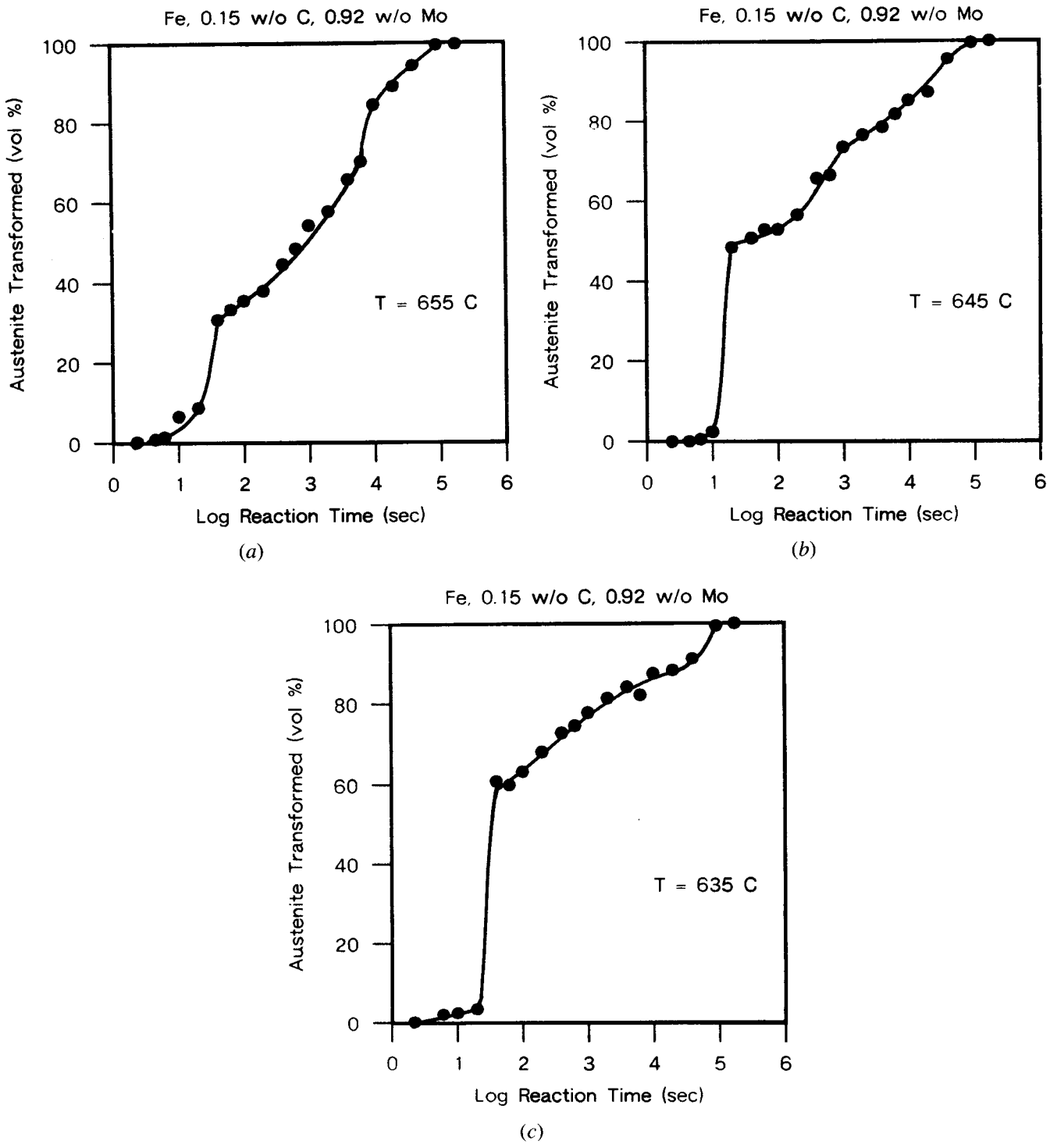

Fig. 10—Isothermal transformation curves for Fe-0.15 wt pct C-0.92 wt pct Mo; the bay temperature is 660 °C: transformed at (*a*) 655 °C, (*b*) 645 °C, and (*c*) 635 °C.

However, available thermodynamic models of austenite do not predict a spinodal reaction.[55] According to another popular view,[56] ferrite embryos of various sizes are suggested to be present during austenitization. Upon quenching to an isothermal reaction temperature, those embryos larger than a critical size transform to bainite by a martensitic mechanism; their growth is again restricted by transformation strain energy. However, it has been shown that embryos cannot be quenched from the austenitizing temperature in Fe-C alloys because of the high diffusivity of carbon in austenite.[57] Furthermore, atom probe experiments have demonstrated the absence of such embryos.[58] Both of these hypotheses were refuted previously by Bradley and Aaronson.[47]

Zener explained the incomplete nature of the bainite reaction in terms of a composition-invariant reaction.[59] Bainite was suggested to form with the same composition as the parent austenite. The C atoms in the highly supersaturated bainite subsequently partition to austenite at higher reaction temperatures; with decreasing

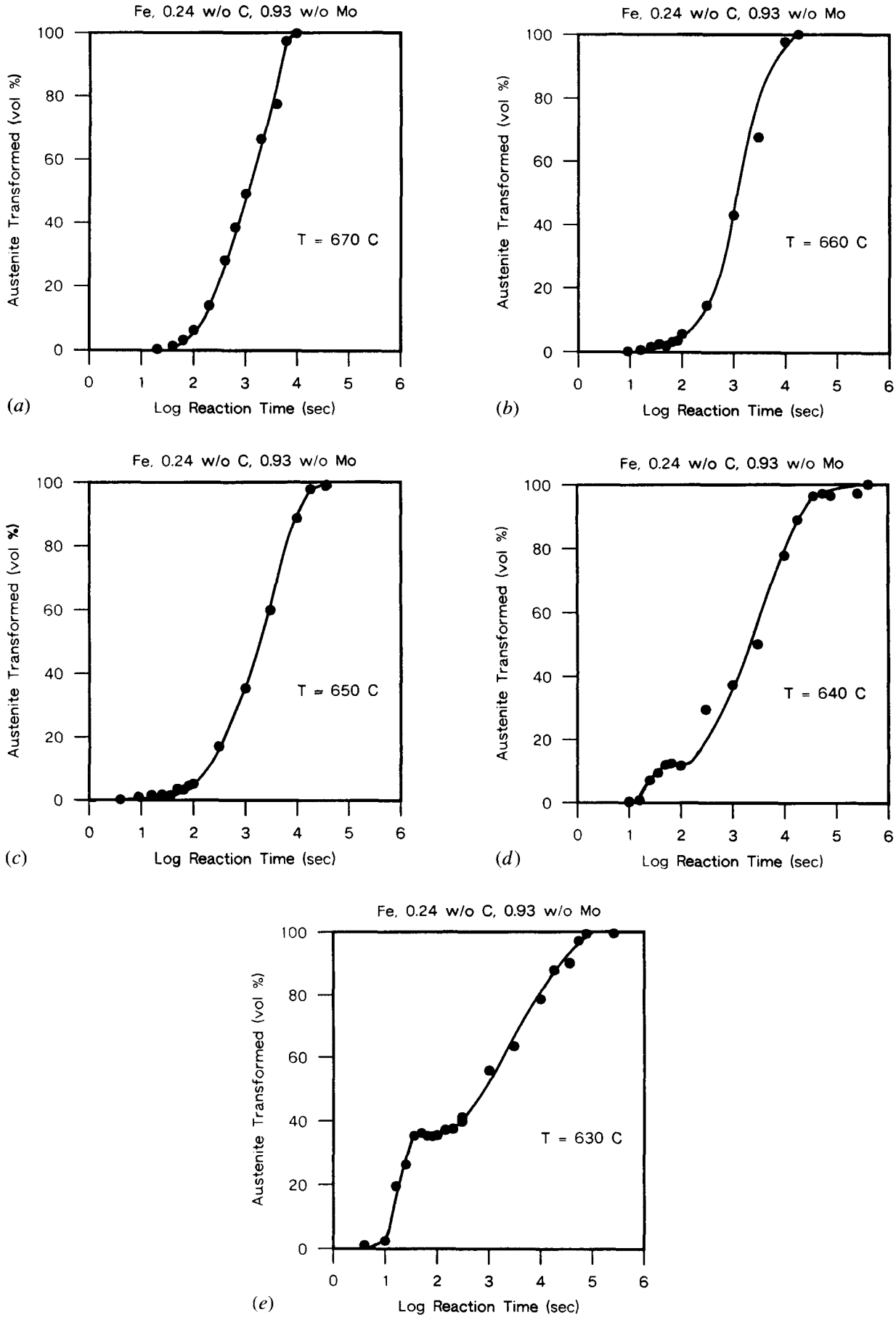

Fig. 11—Isothermal transformation curves for Fe-0.24 wt pct C-0.93 wt pct Mo; the bay temperature is 650 °C: transformed at (*a*) 670 °C, (*b*) 660 °C, (*c*) 650 °C, (*d*) 640 °C, and (*e*) 630 °C.

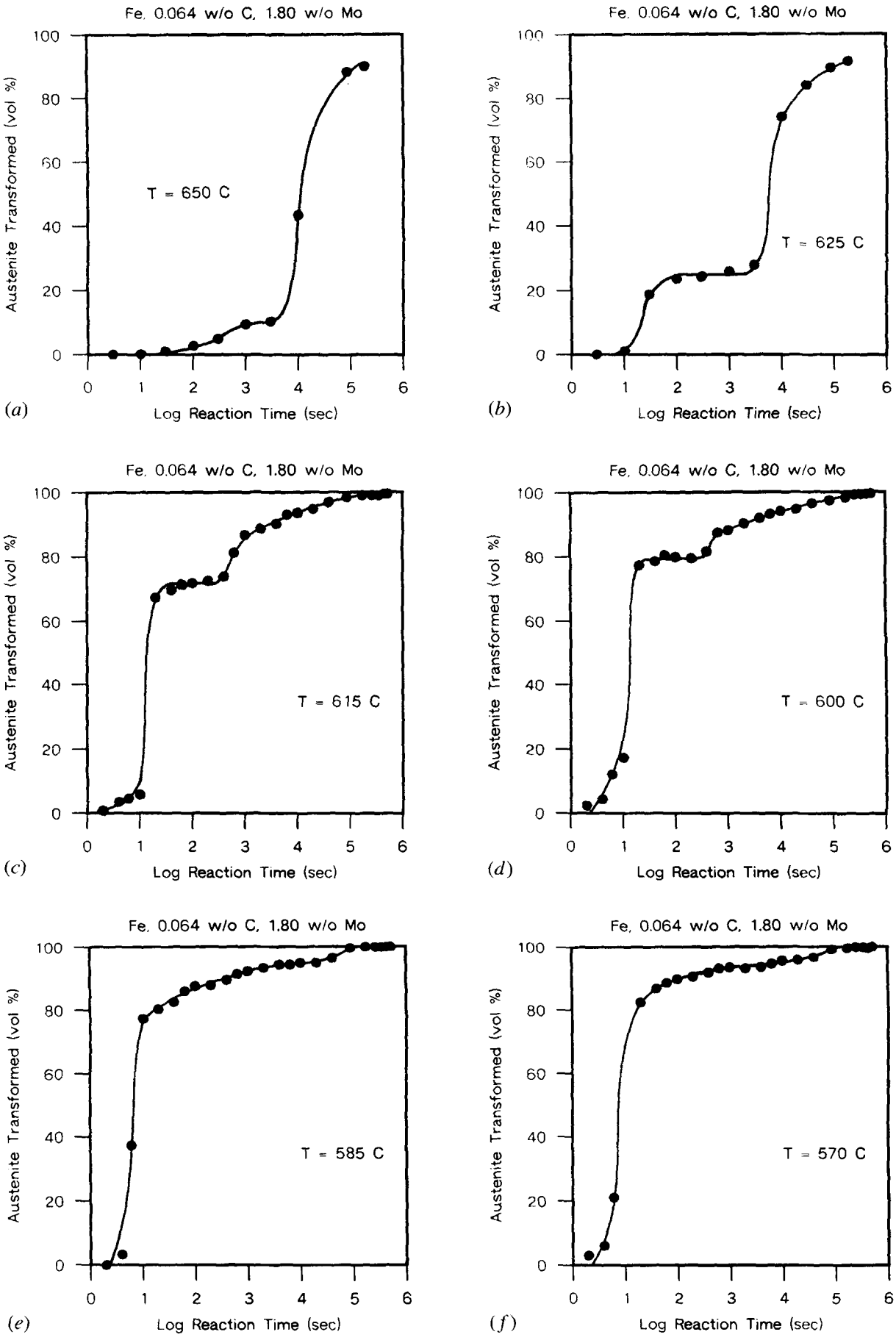

Fig. 12—Isothermal transformation curves for Fe-0.064 *wt* pct C-1.80 *wt* pct Mo; the bay temperature is 655 °C: transformed at (*a*) 650 °C, (*b*) 625 °C, (*c*) 615 °C, (*d*) 600 °C, (*e*) 585 °C, and (*f*) 570 °C.

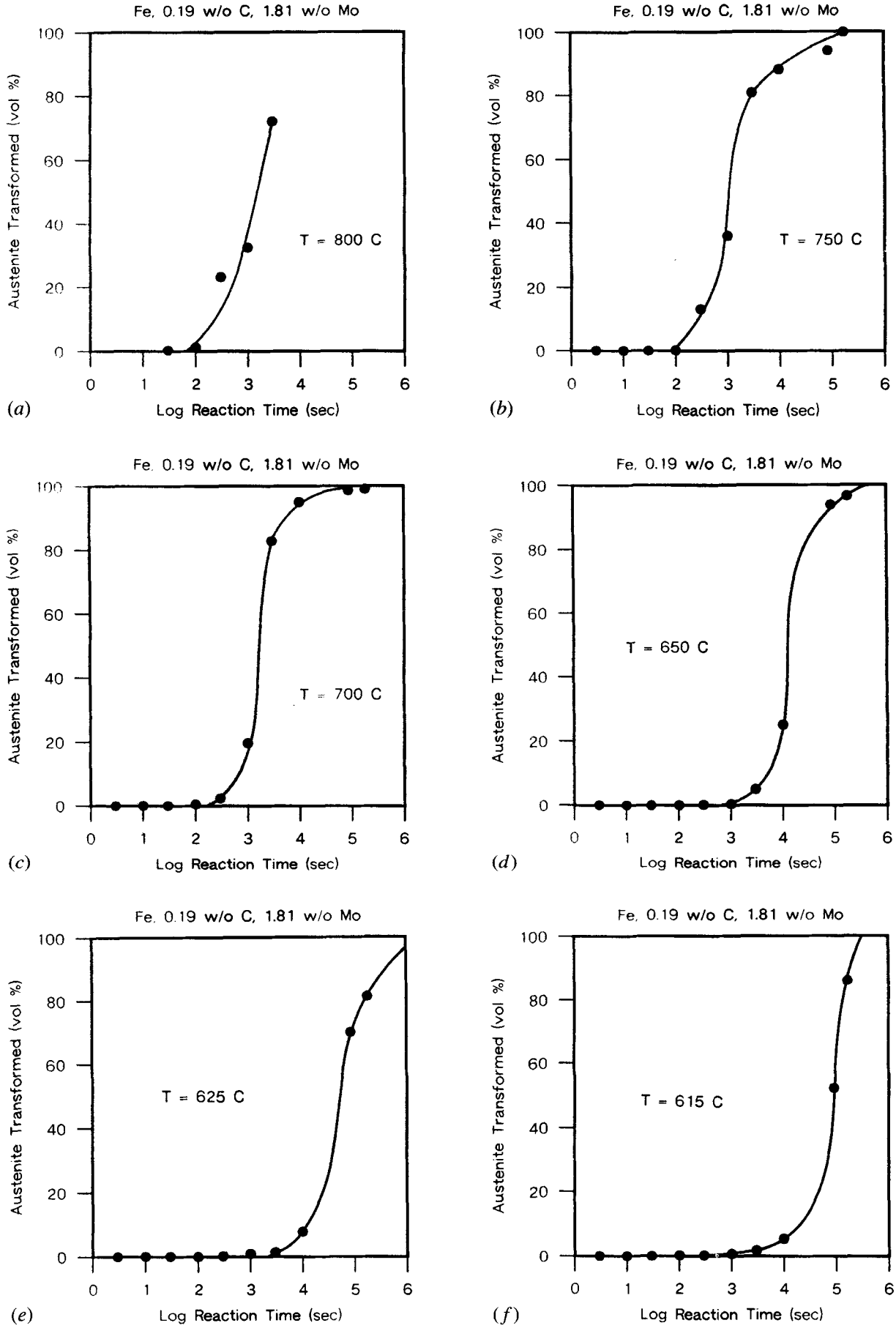

Fig. 13—Isothermal transformation curves for Fe-0.19 wt pct C-1.81 wt pct Mo; the bay temperature is 615 °C: transformed at (*a*) 800 °C, (*b*) 750 °C, (*c*) 700 °C, (*d*) 650 °C, (*e*) 625 °C, (*f*) 615 °C, (*g*) 600 °C, (*h*) 585 °C, and (*i*) 570 °C.

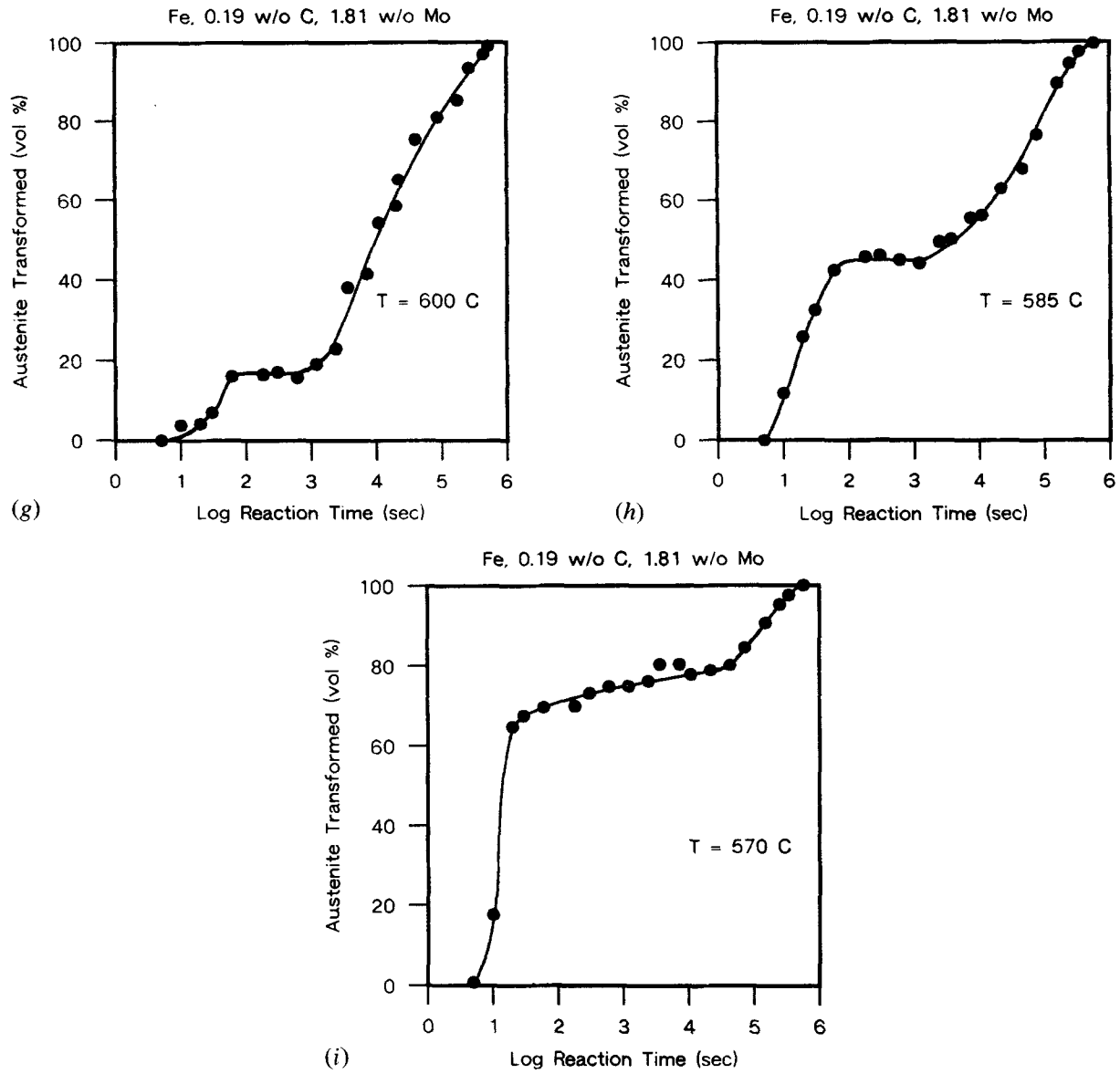

Fig. 13 Cont.—Isothermal transformation curves for Fe-0.19 wt pct C-1.81 wt pct Mo; the bay temperature is 615 °C: transformed at (*a*) 800 °C, (*b*) 750 °C, (*c*) 700 °C, (*d*) 650 °C, (*e*) 625 °C, (*f*) 615 °C, (*g*) 600 °C, (*h*) 585 °C, and (*i*) 570 °C.

temperature, some of the excess carbon is precipitated from ferrite as carbides. As transformation proceeds, the comparatively rapid diffusion of C through the body-centered lattice of the bainite causes the C concentration of the remaining austenite to increase until the free energy change associated with the composition-invariant transformation becomes zero. The upper limiting temperature of the bainite reaction, on this theory, is T_0, the temperature at which austenite and ferrite with the same composition have equal free energies in the absence of strain energy. While the calculated T_0 temperature agrees with the measured kinetic B_s temperature in some steels, the theory fails for others.[41] In addition, the growth of individual crystals in a bainite sheaf occurs at rates consistent with control by carbon diffusion in *austenite*.[41] On the Zener model, which is essentially a massive transformation mechanism, much higher growth rates are expected. Zener[59] also suggested that carbon rejected from growing bainite could cause a film of cementite to form around the bainite. This film could inhibit further bainite growth and result in incomplete transformation. Such a cementite film has not, however, been observed.

On the basis of their observation that bainite formation at a free surface is accompanied by martensite-like upheavals, Ko and Cottrell[27] concluded that the bainite transformation proceeds by a martensitic reaction paced by the diffusion of carbon away from the growing bainite plates. Carbon enrichment of austenite during the transformation is responsible for lowering the driving force for the bainite reaction and for retarding bainite growth. Transformation was proposed to stop when carbides precipitate on the moving ferrite:austenite interphase boundaries, thereby destroying their coherency and their ability to migrate martensitically. However, interfacial structure studies of ferrite and bainite plates have demonstrated that the ferrite:austenite boundaries have a sessile, misfit dislocation structure.[60,61,62] Consequently, bainite cannot form martensitically by the glide of the dislocations in ferrite:austenite boundaries.

Aaronson proposed that the incomplete transformation

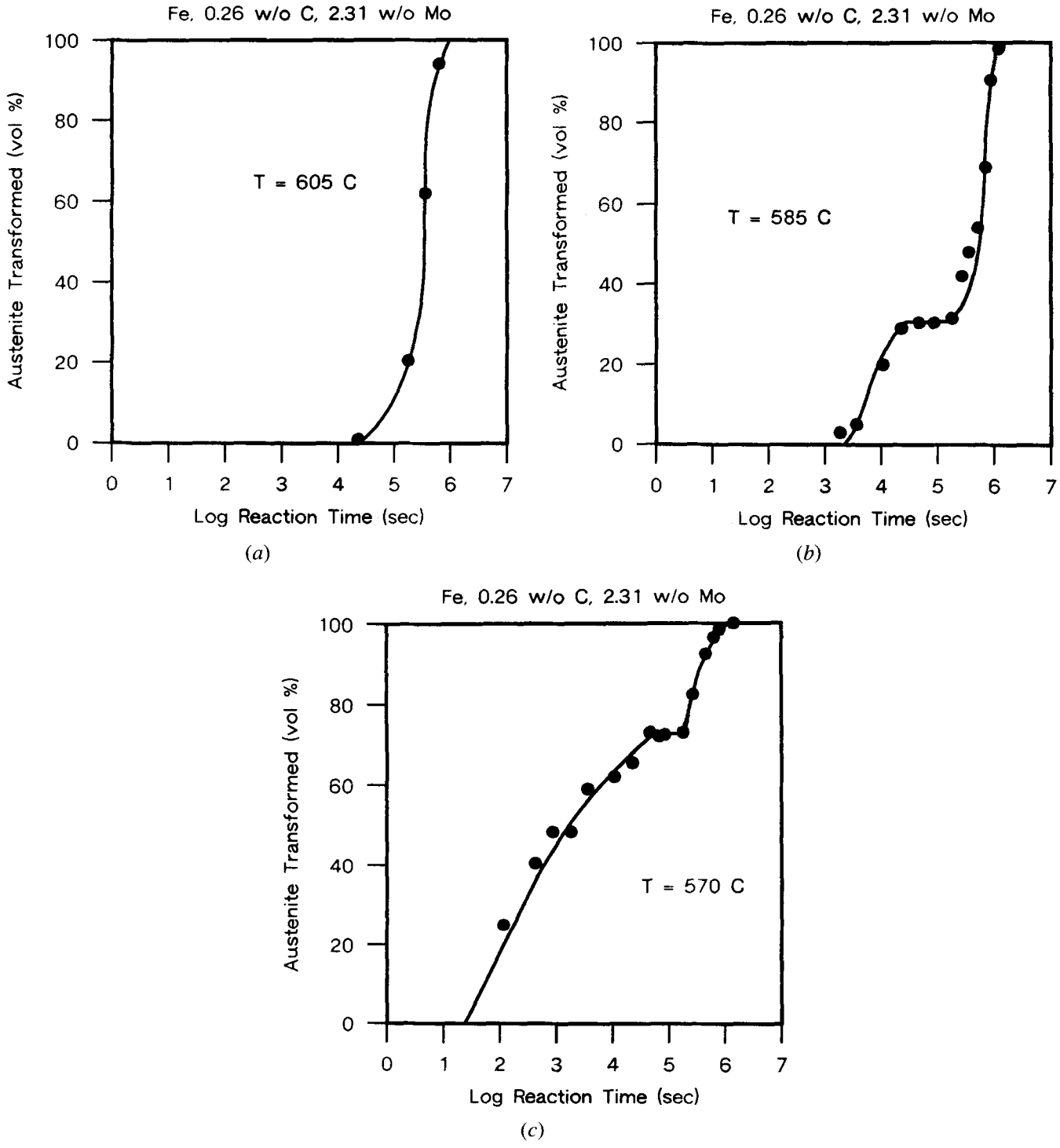

Fig. 14—Isothermal transformation curves for Fe-0.26 wt pct C-2.31 wt pct Mo; the bay temperature is 605 °C: transformed at (*a*) 605 °C, (*b*) 585 °C, and (*c*) 570 °C.

phenomenon is a special effect of certain alloying elements upon the proeutectoid ferrite reaction.[14] It results from a solute drag effect of these alloying elements upon the migration of disordered areas of ferrite:austenite boundaries. On the earliest version of this view,[14,21,22] slow-diffusing substitutional solute atoms which have a negative interaction energy with ferrite:austenite boundaries exert a drag force on these boundaries when the atoms are swept up and briefly retained within the moving boundaries. This approach was an attempt to apply to phase transformations a concept originally developed for grain boundary motion during grain growth.[63-67] The slow growth of ferrite resulting from the solute drag and a similar interference with the evolution of ferrite embryos during nucleation were suggested to cause incomplete transformation.[14] The origin of the drag force was subsequently modified by Bradley and Aaronson,[47] who recognized that substitutional solute diffusion is too sluggish at temperatures of interest for those elements to exert a substantial drag force on the ferrite:austenite

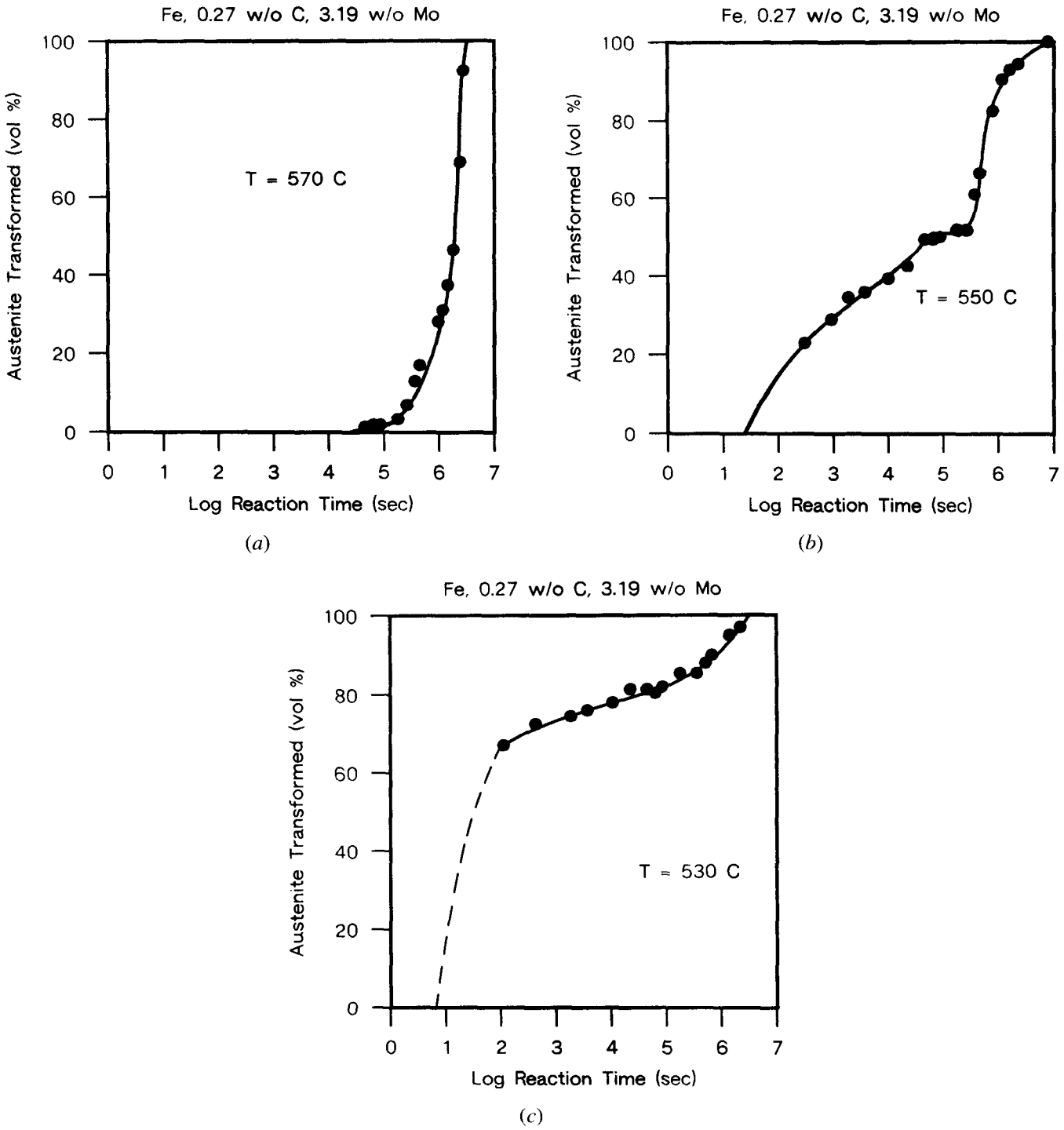

Fig. 15—Isothermal transformation curves for Fe-0.27 wt pct C-3.19 wt pct Mo; the bay temperature is 570 °C: transformed at (*a*) 570 °C, (*b*) 550 °C, and (*c*) 530 °C.

boundaries. On their version, which they termed the "solute drag-*like* effect," substitutional alloying elecments which bind strongly to carbon and which also tend to segregate to ferrite:austenite boundaries, are swept up by the boundary during growth until a steady-state concentration is attained. The adsorbed solute lowers the activity of C in the austenite in contact with the boundary, which, in turn, reduces the activity gradient of C driving diffusion during growth. The substitutional solute concentration in ferrite:austenite boundaries was suggested to increase with decreasing temperature because of both the reduced entropic contribution to segregation and the linear increase in the carbon concentration in austenite corresponding to the extrapolated $\gamma/\alpha + \gamma$ phase boundary. The bay in the TTT diagram was proposed to occur when the ferrite:austenite boundaries become saturated with the substitutional solute and the SDLE is a maximum. Further increases in the driving force for growth then permit recovery of growth kinetics at lower temperatures. Growth stasis occurs when the carbon activity gradient driving growth is eliminated. Shiflet and Aaronson[1] later observed growth stasis in Fe-C-Mo

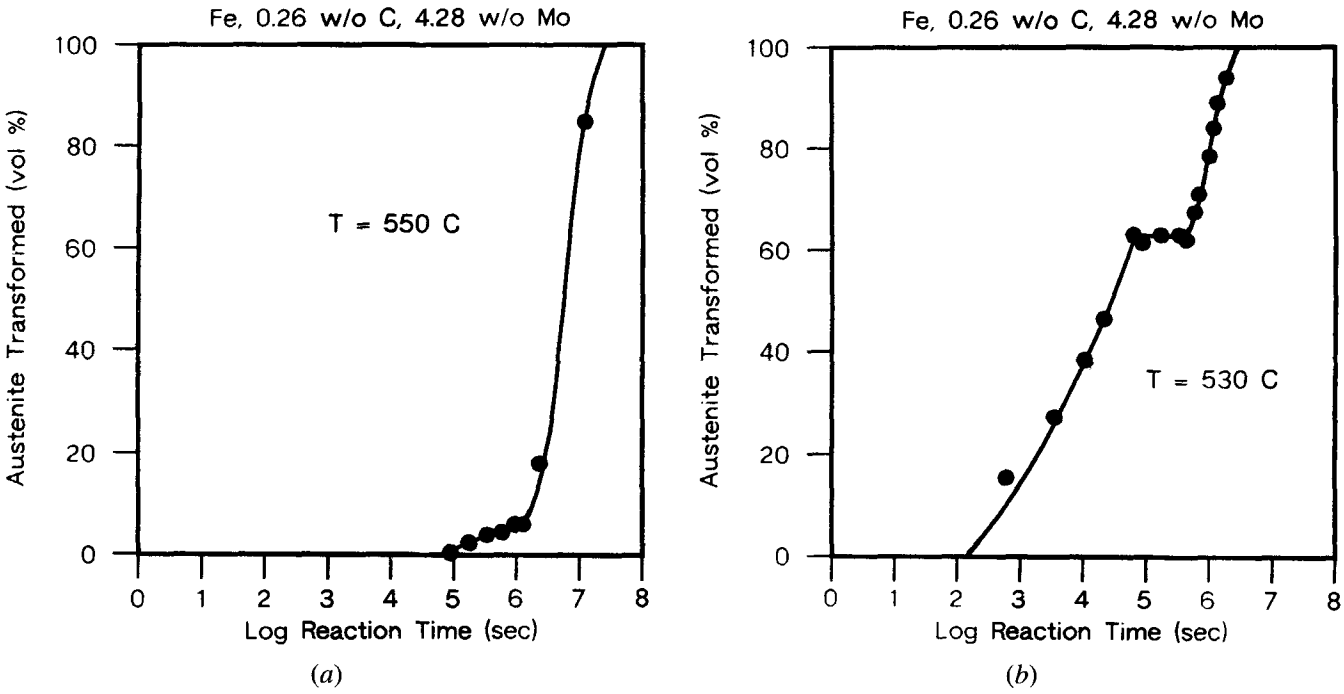

Fig. 16—Isothermal transformation curves for Fe-0.26 wt pct C-4.28 wt pct Mo; the bay temperature is 550 °C: transformed at (*a*) 550 °C and (*b*) 530 °C.

alloys at temperatures above T_b but noted that the cessation of growth is a temporary condition. The (microstructural) bainite transformation resumes following growth stasis. This was attributed to a reduction in the SDLE resulting from either the diffusion of excess Mo away from $\alpha:\gamma$ boundaries or the precipitation of this Mo as an alloy carbide.

The SDLE was also suggested to be responsible for the absence of the Widmanstätten morphology in Fe-C-Mo alloys at reaction temperatures between the upper nose and the bay in the TTT diagram.[22] Preferential adsorption of Mo at the disordered areas of $\alpha:\gamma$ boundaries causes the SDLE to be strongest at the most mobile portions of the boundaries. This results in a decrease in the anisotropy of growth and can account, at least partially, for the absence of ferrite plates at temperatures above T_b in Fe-C-Mo alloys.

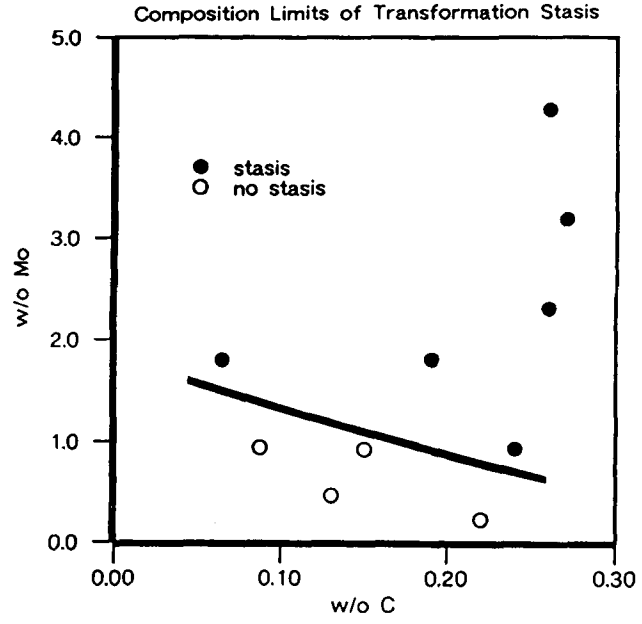

Fig. 17—Carbon and molybdenum concentrations of Fe-C-Mo alloys which do or do not exhibit transformation stasis below the bay temperature.

Experimental data on the growth kinetics of ferrite allotriomorphs provide some support for the SDLE hypothesis. As was mentioned earlier, the growth kinetics of ferrite in Fe-C-Mo alloys pass through a maximum near the upper nose in the TTT diagram[21] and minimum near the bay temperature.[19] In addition, the ferrite and ferrite + carbide mixtures formed at and above the bay temperature in Fe-C-Mo alloys exhibit as many as three distinct stages of growth with time.[1] These growth stages are arranged in the four patterns shown schematically in Figure 19(a).[1] The C and Mo concentrations of alloys which exhibit these types of behavior are shown at the bay temperature (Figure 19(b)), 20 °C above T_b and 40 °C above T_b (Figures 19(c) and (d), respectively, of Reference 1). None of these observations can be explained by currently available growth models. Slower than predicted ferrite growth kinetics have also been reported in an Fe-C-Cr alloy at reaction temperatures above T_b.[47]

In view of these data and the failure of alternate explanations for the incomplete transformation phenomenon, the SDLE appears to be at least a reasonable approach to understanding the kinetic features of bainite emphasized in the overall reaction kinetics definition of bainite. The next section will discuss results of the present investigation in terms of the SDLE hypothesis, and the last section will outline a further developed, and further altered, model for this effect.

A. *Overall Transformation Kinetics*

The interpretation to follow of the transformation kinetics behavior observed during the present investigation

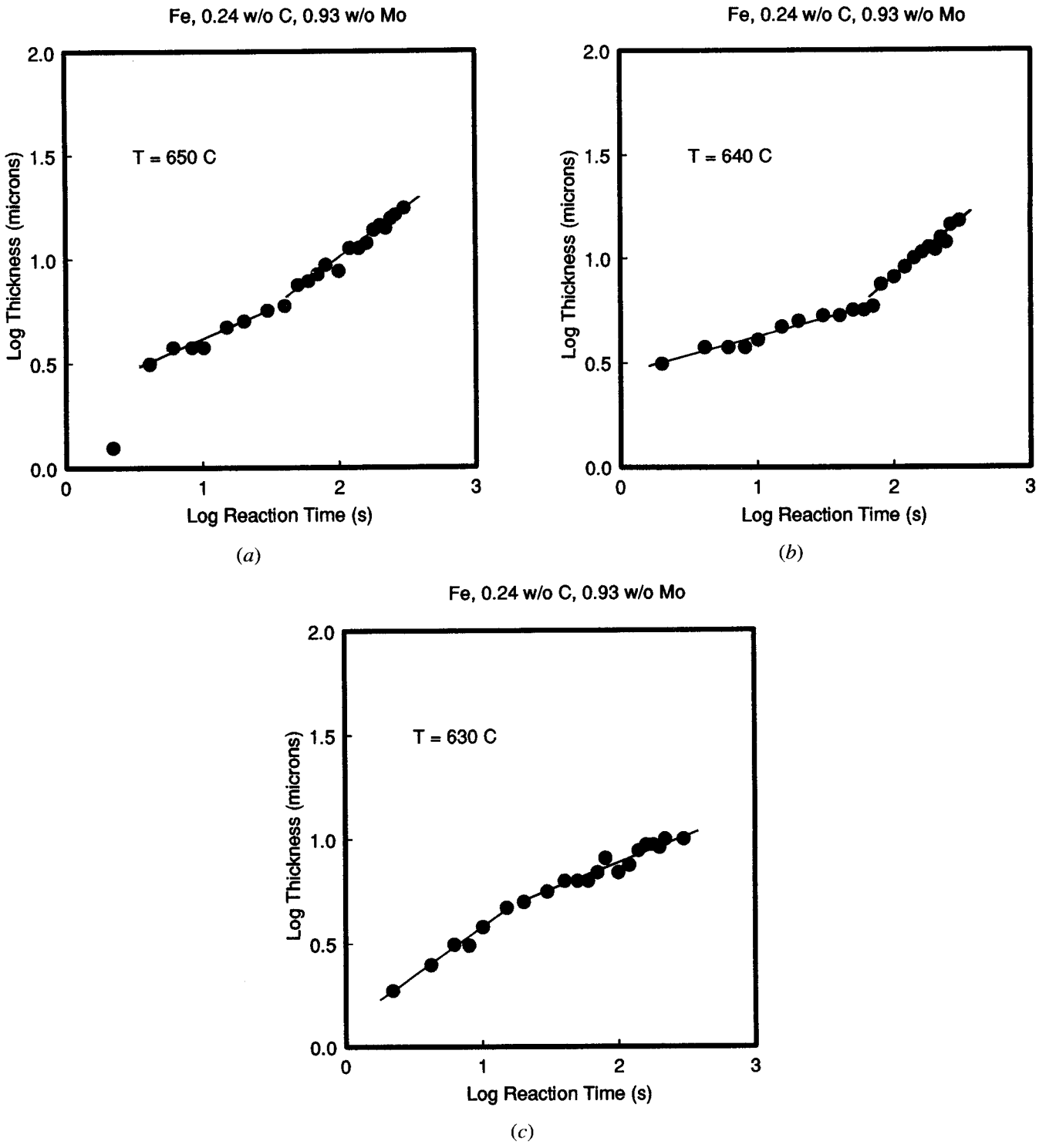

Fig. 18—Thickening kinetics of grain boundary allotriomorphs in Fe-0.24 wt pct C-0.93 wt pct Mo: transformed at (*a*) 650 °C (the bay temperature), (*b*) 640 °C, and (*c*) 630 °C.

is based primarily upon the SDLE hypothesis. However, one aspect of this hypothesis will first be altered, a further consideration will be added, and a confirmation of a proposed mechanism for the reduction of the SDLE[1] will be discussed. The portion of the SDLE hypothesis to be changed is that which postulates that disordered areas of ferrite:austenite boundaries are saturated with substitutional solute at the bay temperature. A recent FIM/AP study of the composition of $\alpha:\gamma$ boundaries in an Fe-0.19 wt pct C-1.81 wt pct Mo alloy reacted at 585 °C for 30 seconds, a temperature about 30 °C below T_b, indicates that ferrite:austenite boundaries are enriched in Mo by a factor of 2. This is about tenfold less than the equilibrium enrichment expected at this temperature for ferrite:ferrite[68] and austenite:austenite[69] boundaries and probably for ferrite:austenite boundaries as well. Nevertheless, since no bulk partition of Mo occurs between austenite and ferrite during growth,[19] the measured twofold enrichment does appear to be significant even though it is far below boundary saturation.

Table II. Ferrite Growth Kinetics in Fe-0.24 Wt Pct C-0.93 Wt Pct Mo, T_b = 650 °C ($S = \alpha t^n$)

	α Experimental ($\mu m/s^{1/2}$)	α Predicted for Paraequilibrium ($\mu m/s^{1/2}$)	n Experimental ($\mu m/s^{1/2}$)	n Predicted for Paraequilibrium ($\mu m/s^{1/2}$)
650 °C				
Stage 1	2.10	2.10	0.28 ± 0.02	0.5
Stage 2	1.14	—	0.47 ± 0.02	—
640 °C				
Stage 1	2.74	2.13	0.19 ± 0.01	0.5
Stage 2	0.78	—	0.51 ± 0.04	—
630 °C				
Stage 1	1.29	2.15	0.46 ± 0.03	0.5
Stage 2	2.21	—	0.27 ± 0.02	—

The consideration is next added to the SDLE hypothesis that when the combination of the SDLE and decreasing reaction temperature has sufficiently reduced ferrite growth kinetics, sympathetic nucleation[39,40] of new ferrite crystals takes place at ferrite:austenite boundaries at rates which increase rapidly with further reductions in reaction temperature. The temperature at which the sympathetic nucleation rate of ferrite becomes significant corresponds to T_b. The degeneracy of ferrite below T_b can be seen to derive from extensive sympathetic nucleation (Figure 6(a)).

Once a ferrite crystal is nucleated, its growth rate diminishes with time. This results in part from the carbon enrichment of austenite in advance of the growing ferrite. Two other possible sources for the declining growth rate arise from the presence of a substitutional solute. First, the X element may decrease the formation kinetics of ferrite growth ledges. This possibility could not be studied in this investigation due to the usual difficulties associated with retaining the austenite in contact with $\alpha:\gamma$ interfaces at room temperature in low-alloy steels. The second source is the operation of the SDLE.[1] On a ledgewise growth mechanism, a decrease in the velocity of a migrating $\alpha:\gamma$ boundary[70,71] is equivalent to an increase in the mean time the partially coherent terraces of the boundary "survive" before being overrun by the carbon diffusion fields associated with the risers of succeeding growth ledges. The supersaturation for ferrite formation at the terraces then increases to the level where sympathetic nucleation can occur again. This process should result in accelerated transformation kinetics below T_b. These repeated, temporary "evasions" of the SDLE are expected to continue until the rising proportion of carbon in the untransformed austenite reduces the driving force for sympathetic nucleation even at the terraces between widely separated risers.

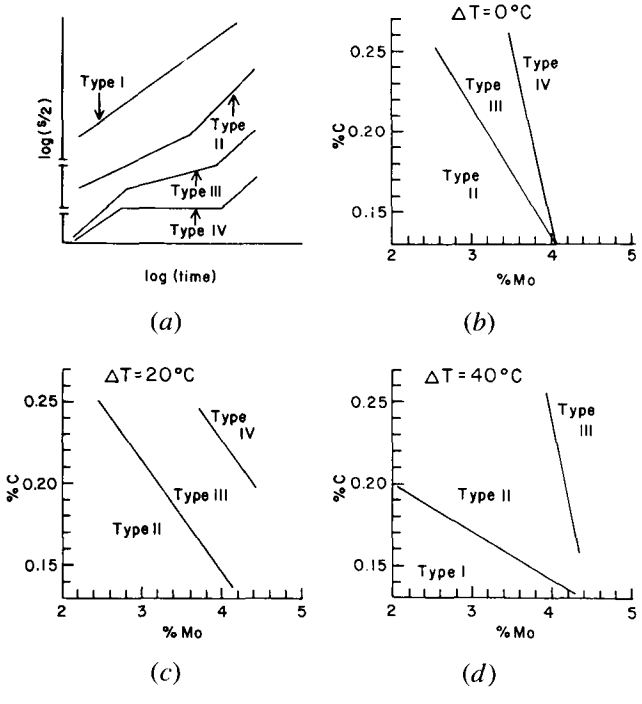

Fig. 19—Allotriomorph thickening kinetics at temperatures above the bay:[1] (*a*) schematic of the four types of growth kinetics and (*b*) carbon and molybdenum ranges which exhibit the different growth types at the bay temperature, (*c*) 20 °C above the bay temperature and (*d*) 40 °C above the bay temperature.[1]

Transformation stasis occurs when the SDLE is strong enough to produce growth stasis of the individual sympathetically nucleated ferrite crystals, and the *local* carbon concentration in austenite at the stationary portions of the ferrite:austenite boundaries remains high enough to make the sympathetic nucleation of new ferrite crystals occur at negligible rates. The latter condition depends on the volume and the distribution of the ferrite that has already been formed and on the reaction temperature. At small undercoolings below T_b, the small loss of supersaturation at the immobile portions of $\alpha:\gamma$ boundaries accompanying the formation of a small quantity of ferrite is sufficient to terminate sympathetic nucleation. At lower reaction temperatures, the driving force for ferrite formation is higher, and a larger volume of ferrite can form before sympathetic nucleation ends. Thus, when transformation stasis occurs, the volume fraction of ferrite present during stasis increases with decreasing temperature from a value of zero at T_b. When the second transformation stage has finite kinetics (*i.e.*, transformation stasis is absent), either the SDLE is not strong enough to produce growth stasis or the sympathetic nucleation rate of ferrite does not reach zero before the initiation of carbide precipitation. Since transformation stasis is associated with carbide-free ferrite, the present results suggest that neither upper nor lower bainite, which are distinguished by their carbide distributions, should exhibit transformation stasis.

It was observed during this investigation that the precipitation of carbides initiates the third stage of transformation. This confirms that ferrite:austenite boundaries can escape growth stasis by the precipitation of carbides at these boundaries, in agreement with an earlier suggestion.[1] Carbide precipitation can have two effects on the transformation kinetics. First, since the carbides are generally alloy carbides precipitated on $\alpha:\gamma$ boundaries, they "getter" the Mo adsorbed on these boundaries and thereby reduce the SDLE. Second, they locally reduce the C content of the parent austenite and increase the driving force for further ferrite growth. Both effects result in an acceleration of the overall transformation kinetics.

With these modifications and considerations, the SDLE mechanism can be employed to explain the features of the overall transformation kinetics at reaction temperatures above and below the bay in the Fe-C-Mo alloys investigated so far. At temperatures above T_b, ferrite nucleation is confined to austenite grain boundaries and twin boundaries, and the SDLE suppresses the formation of Widmanstätten ferrite. At these temperatures, ferrite nucleation does not cease until after growth stasis ends. Consequently, the nucleation rate and the growth rate of ferrite are not zero at the same time, and transformation stasis does not occur. The transformation curves at temperatures above T_b thus have a sigmoidal shape (Figure 5(a)). Below the bay, the increased driving force for ferrite formation causes the austenite grain and twin boundary nucleation sites to saturate quickly. Ferrite nucleation can continue at $\alpha:\gamma$ boundaries, however, and will proceed until the austenite surrounding the newly formed ferrite crystals becomes too enriched with carbon to support further sympathetic nucleation. When this happens concurrently with growth stasis, transformation stasis is observed.

The absence of Widmanstätten ferrite above the bay may be due to the SDLE, as previously noted, or due to the precipitation of Mo carbides during the early stages of transformation on the following rationale. Plates are expected to develop when there is a significant anisotropy of interfacial boundary mobility.[37] Boundary orientations which result in substantial areas of partial coherency (*e.g.*, the broad faces of plates) are less mobile than boundaries which have a higher density of sites where atomic attachment is feasible (*e.g.*, the edges of plates).[37] However, the stationary portions of the boundary, *i.e.*, the terraces of ledges, are the most likely sites for carbide nucleation.[72,73] Carbide precipitation at the slower moving boundary orientations increases the competitive advantage of these boundaries relative to the faster moving boundary orientations in two ways.[43] First, the precipitation of carbides locally increases the driving force for ferrite growth.[43] Second, the ferrite:carbide:austenite junctions may provide favorable sites for the formation of additional ferrite growth ledges.[43] Thus, the precipitation of fine alloy carbides at $\alpha:\gamma$ boundaries can reduce the anisotropy of ferrite growth and favor the development of an allotriomorphic reaction product. This explanation has also been used to explain the development of the equiaxed nodular bainite structure formed during the latter stages of austenite decomposition in Fe-C-Mo alloys.[25]

The transformation sequence below T_b is shown schematically in Figure 20. Ferrite nucleation begins at austenite grain boundaries, but sympathetic nucleation results in transformation developing preferentially toward the grain interiors rather than along the austenite grain boundaries. Saturation of the nucleation sites does not occur in this circumstance. On the contrary, the formation of new ferrite crystals increases the total ferrite:austenite boundary area and thereby creates additional nucleation sites. Since nucleation kinetics tend to vary sharply with temperature, a small decrease in reaction temperature below T_b yields markedly increased sympathetic nucleation kinetics. The initial growth kinetics of ferrite in the presence of an SDLE have been shown to be relatively rapid.[1] Hence, the repeated nucleation occurring below T_b results in higher ferrite growth kinetics when averaged over many crystals than at temperatures above the bay, where repeated nucleation is absent and ferrite growth kinetics decrease with time.[1] The combination of a higher nucleation rate and a higher effective growth rate of ferrite yields greatly accelerated overall transformation kinetics at reaction temperatures below T_b. The increased ferrite growth rate also inhibits carbide nucleation at $\alpha:\gamma$ boundaries by decreasing the mean survival time of the terraces between passing growth ledges. The passage of successive risers across terraces of $\alpha:\gamma$ boundaries thus becomes too frequent to allow the carbide phase time to nucleate. As a further consequence of the accelerated transformation kinetics, extensive overlap of the carbon diffusion fields of neighboring ferrite crystals soon occurs, as earlier described. The resulting carbon enrichment of the remaining austenite causes a cessation of sympathetic nucleation and the initiation of a second transformation stage with slower overall kinetics.

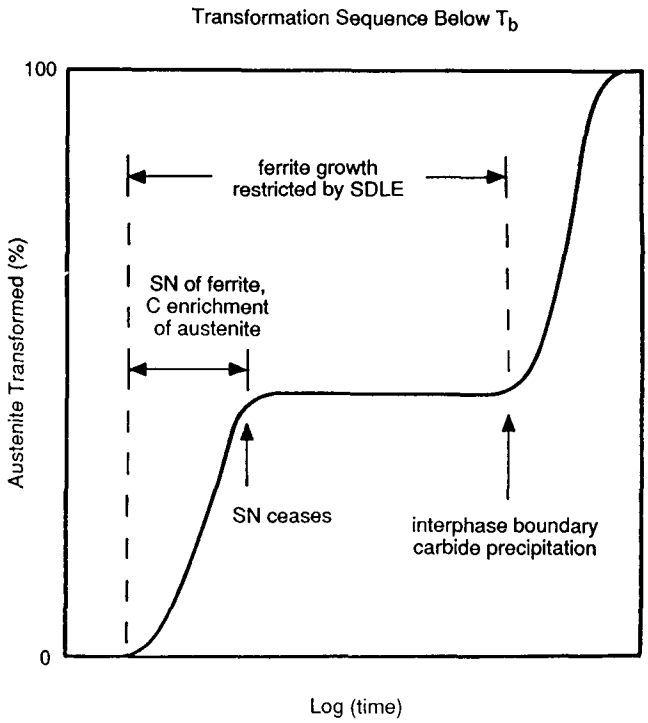

Fig. 20—Schematic representation of the transformation sequence at temperatures below T_b.

Once sympathetic nucleation ceases, any increase in the ferrite volume fraction must occur by growth of existing ferrite crystals. Because ferrite growth is restricted by an SDLE, the overall transformation kinetics during the second stage are greatly reduced relative to those of the first stage. If the SDLE is strong enough to induce ferrite growth stasis, then the second stage corresponds to overall transformation stasis, provided that ferrite nucleation at austenite grain boundaries (and at intragranular sites wholly within austenite) has also stopped. If, on the other hand, ferrite growth does not cease entirely, transformation stasis does not occur, and the second transformation stage has a slightly positive slope. This condition can result when the Mo and/or C concentrations in the alloy are sufficiently low, or the driving force for ferrite growth is sufficiently high.

The third stage begins with the precipitation of interphase boundary carbides. Growth of the ferrite + carbide mixture during the third stage is more nearly equiaxed, much like growth at temperatures above the bay. Carbide precipitation at ferrite:austenite boundaries is, in the context of ferrite growth kinetics, a process antithetical to the SDLE, since it should drain the SDLE-producing alloying element from $\alpha:\gamma$ boundaries. Because elements which produce an SDLE in Fe-C-X alloys often promote carbide precipitation, the development of transformation stasis seems to depend in an inverse manner upon the kinetics of carbide precipitation. There are at least two ways in which the formation of carbides can be postponed long enough for stasis to develop. In Fe-C-Mo, and perhaps in other Fe-C-X alloys as well, the rapid initial growth kinetics of sympathetically nucleated ferrite below T_b inhibit carbide precipitation at ferrite:austenite boundaries, as described previously. The increased difficulty of alloy carbide precipitation with decreasing reaction temperature accentuates this effect. The use of synergistic combinations of alloying elements is a second approach to delaying carbide precipitation long enough for transformation stasis to occur.[26] For example, the combination of one alloying element which produces an SDLE, *e.g.*, Mo or Mn, with a second element which inhibits carbide precipitation, *e.g.*, Si, may result in an alloy in which the SDLE is free to encourage sympathetic ferrite nucleation of ferrite and subsequent transformation stasis without interference from carbide precipitation. The synergism giving rise to transformation stasis in such steels could also result from an increase in the SDLE of one alloying element due to the presence of the second element.[74]

In low-Mo alloys, the three-stage transformation behavior is not observed (Figure 7). The absence of a second transformation stage can be attributed to the fact that the SDLE is not strong enough at low Mo levels to halt the growth of ferrite. Once nucleated, the ferrite can develop into the plate or lath morphology characteristic of Fe-C alloys and low-alloy steels. This composition dependence of the SDLE is indirectly, but usefully, supported by a comparison of the degenerate ferrite morphology in an alloy in which the SDLE is strong (Figure 2(b)) with the ferrite morphology in an alloy containing less Mo in which the SDLE is presumably weaker (Figure 2(c)). The morphology of ferrite in Figure 2(c) is more nearly as it appears in Fe-C alloys.

The effect of the C concentration in the alloy is most evident in the 0.9 pct Mo alloys (*cf.* Figures 9, 10, and 11). At this level of Mo, increasing the C concentration has the effect of inducing transformation stasis during the second stage. A second stage is not apparent in the 0.086C alloy (Figure 9); the 0.15C alloy has a distinct second stage but no transformation stasis (Figure 10), and the 0.24C alloy exhibits a short but discernible period of transformation stasis (Figure 11). In the lower C alloy, loss of supersaturation attending the overlap of carbon diffusion fields is not severe enough to inhibit sympathetic nucleation. The nucleation process can thus continue, at least until carbide precipitation begins. In the 0.24C alloy, supersaturation loss through diffusion field overlap is extensive enough to prevent sympathetic nucleation, and transformation stasis occurs before carbides are able to precipitate.

The combined effects of the Mo concentration and the temperature upon the development of transformation stasis at a constant C concentration of about 0.2 pct are summarized in Figure 21. The upper temperature limit of the stasis region corresponds to the temperature of the bay. Since sympathetic nucleation of ferrite during the first transformation stage is a prerequisite for the development of a second stage, transformation stasis can only occur below T_b. The lower temperature limit of the stasis region is the temperature below which the slope of the second stage of transformation becomes greater than zero. This results from the continued nucleation and/or growth of ferrite at temperatures low enough so that the SDLE can be overcome by the increasing driving force for ferrite formation. The disappearance of transformation stasis below approximately 1 pct Mo (see Figure 17 at 0.2 pct C) is due to the relatively unrestricted growth of ferrite resulting from the diminished strength of the SDLE.

It is worthwhile to note that the gradual disappearance of transformation stasis with decreasing temperature

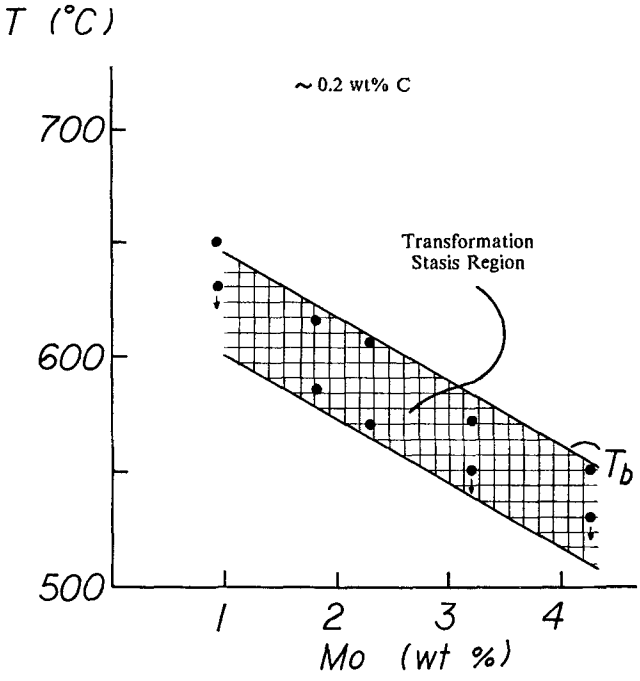

Fig. 21—The effect of Mo concentration (at 0.2 wt pct C) on the temperature range for transformation stasis.

contradicts the view that the bainite reaction has a distinct B_f, occurring at a volume fraction of unity analogous to the martensite finish temperature.[13] At least in the present alloys, this is not observed. For example, with decreasing temperature, transformation stasis disappears between 570 °C and 585 °C in the Fe-0.19C-1.81Mo alloy (Figure 13), yet the proportion of ferrite at the beginning of the second stage of transformation at 570 °C is still much less than unity. The bainite/martensite parallel is further weakened by the fact that incomplete transformation is not observed in low-Mo, low-C alloys (Figure 17). In Fe-C base alloys, however, both M_s and M_f temperatures are readily delineated over the widest accessible ranges of C concentration. Thus, the lower bound of the transformation stasis region in Figure 21 does not represent the B_f temperature as usually defined.

B. *Growth Kinetics*

Previous investigations of the growth kinetics of bainite have usually emphasized the lengthening and thickening rates of bainite plates.[41,75–81] However, strong interfacial structure barriers to the growth of plate-shaped precipitates[81–84] complicate the interpretation of such data. While this barrier to growth evidently also occurs at grain boundary allotriomorphs,[85] it appears to be less effective, presumably due to the higher average density of ledges on allotriomorph interphase boundaries. When measured properly,[34,47] allotriomorph thickening kinetics can yield reproducible data with which to investigate the SDLE of alloying elements; corrections for structural barriers to growth are generally minor.[34,47]

Previous studies of allotriomorph thickening in Fe-C-Mo alloys have demonstrated significant discrepancies between experimentally determined ferrite growth kinetics and those calculated assuming paraequilibrium growth with either a planar or an ellipsoidal interface and control of growth by carbon diffusion in austenite away from a disordered $\alpha:\gamma$ boundary.[1,19,21] Neither the observed maximum in the growth kinetics at the upper nose of the TTT diagram[21] nor a minimum in the kinetics at the bay temperature[19] are predicted by any currently available growth model. A number of qualitative explanations for these discrepancies have been proposed, including the transition from orthoequilibrium to paraequilibrium growth,[86] carbon clustering, GP (Guinier-Preston) zone formation or carbide precipitation within austenite,[87,88] and pinning of ferrite: austenite boundaries by carbides.[88,89] These explanations have been ruled out previously as primary sources for the differences between measurements and calculations.[47] Additional complications in ferrite growth behavior have been found by Shiflet and Aaronson.[1] Whereas previous studies almost invariably yielded parabolic thickening kinetics of ferrite allotriomorphs, these investigators observed that allotriomorph thickening in alloys containing 0.15 to 0.25 pct C and 2.3 to 4.3 pct Mo can exhibit up to four different types of kinetics (Figure 19 of Reference 1) at temperatures above T_b.[1] These stages depend on the C and Mo concentrations and the reaction temperature.[1] During the middle stage of Type IV growth (Figure 19 of Reference 1), allotriomorph thickening ceases entirely; this phenomenon was termed growth stasis.[1] Examples of growth stasis have also been observed in Fe-C-Mo alloys with hot-stage, high-voltage electron microscopy by Purdy.[88]

The present work indicates that at least some of the growth types found in Fe-C-Mo alloys above T_b also occur below T_b. The two-stage growth observed in Fe-0.24C-0.93Mo at 650 °C (T_b) and 640 °C (Figures 18(a) and (b)) falls into the Type II category of Figure 19, in which the second stage of growth has a steeper slope (in the log of thickness *vs* log t plot) than the first. At 630 °C, however, the second stage has slower kinetics than the first. This may be due to "soft impingement" (significant overlap of the C diffusion fields associated with adjacent ferrite crystals) or to the appearance of only the first two stages of Type III growth prior to termination of the measurements. The former possibility is eliminated by comparing the extent of the C diffusion field around a growing ferrite crystal to the average distance between such crystals. Growth measurements at 630 °C were terminated when the fraction of intragranular degenerate ferrite had increased to the point where sampling of grain boundary ferrite allotriomorphs became difficult. This occurred at an allotriomorph thickness of about 10 μm; nearest-neighboring ferrite crystals were at least 20 μm away. Applying Zener's linearized gradient analysis[46,90] to this alloy and temperature on the paraequilibrium assumption, the C diffusion field extends less than 1 μm from a spherical ferrite precipitate 10 μm in diameter or approximately 5 μm from the "worst case" estimate of a 10-μm-thick ferrite crystal with a planar growth front. Therefore, the decrease in growth kinetics at 630 °C occurs well before significant overlap of C diffusion fields. The growth behavior at this temperature thus appears to be an example of the Type III growth mode, as would be expected[1] on the basis of the lower reaction temperature.

Type IV allotriomorph thickening kinetics, whose middle stage corresponds to growth stasis, were not found at T_b (650 °C) or up to 20 °C below T_b in the Fe-0.24C-0.93Mo alloy. This seems to disagree with the observation that this alloy exhibits *transformation* stasis at 640 °C and 630 °C (Figures 11(d) and (e)). However, this discrepancy is due to the fact that the growth measurements were made on grain boundary allotriomorphs, which account for only a small proportion of the ferrite formed at temperatures below T_b. Most of the ferrite at these temperatures is of the degenerate variety, composed of small, sympathetically nucleated crystals, which evidently *do* achieve growth stasis. The small increase in the amount of ferrite resulting from the formation of allotriomorphs is less than the error in the quantitative metallographic determination of the ferrite volume fraction and, thus, should have little effect on the overall transformation kinetics below T_b. Unfortunately, the irregular shapes of the degenerate structures prevent useful measurements from being made on their growth kinetics. Some form of hot-stage microscopy may be required in order to test our conclusion that the degenerate morphology undergoes the predicted growth stasis.

As to why ferrite crystals comprising degenerate structures almost certainly exhibit growth stasis while grain boundary allotriomorphs do not, one can no longer ascribe this distinction to gross differences in interphase

boundary structure. A recent investigation of the interfacial structure of grain boundary α allotriomorphs in a hypoeutectoid Ti-Cr alloy shows that these boundaries are partially coherent at both their rationally *and* irrationally oriented interfaces.[85] This observation indicates that the interphase boundary structures of plates[22,91] and allotriomorphs are basically similar. However, the relatively complex shapes of even individual crystals within degenerate plates suggest that their growth ledge structures are more complicated and diverse than those on allotriomorphs. This is contrary to normal expectation and perhaps arises from the important role which sympathetic nucleation plays in the development of degenerate Widmanstätten structures. In Ti-base alloys, the precipitate:precipitate interfaces created during sympathetic nucleation have been found to be a good source of growth ledges,[40] and degenerate plates have been shown to be associated with a particularly complex ledge structure.[92]

A further explanation for the different growth kinetics of these two morphologies is that degenerate ferrite crystals, particularly at later stages of transformation, are growing into austenite containing an appreciably higher carbon concentration than the bulk carbon content. On the other hand, allotriomorph thickening measurements are deliberately made prior to overlap of C diffusion fields from neighboring ferrite crystals. Ferrite growth kinetics decrease, and the SDLE appears to become more effective with increasing bulk carbon concentration, *i.e.*, as the supersaturation driving growth decreases.[93] Hence, the development of growth stasis in association with degenerate ferrite (rather than allotriomorphs) is promoted by the lesser supersaturation into which degenerate ferrite grows.

C. *Solute Drag-Like Effect*

In this section, an attempt will be made to place the SDLE, upon which most of the preceding sections have been based, on a more quantitative basis and to apply it to experimental data we have reported on the composition of ferrite:austenite boundaries in an Fe-C-Mo alloy.[94] The underlying assumptions of the model to be developed are as follows. The growth of carbide-free ferrite with an SDLE occurs without bulk partitioning of substitutional alloying elements between austenite and ferrite. This requirement is met by most alloying elements at temperatures almost up to the Ae3[55] and has been demonstrated in Fe-C-2 pct Mo alloys with both electron microprobe[19] and FIM/AP[94] analysis. Furthermore, ferrite growth kinetics are taken to be approximated adequately as controlled by carbon diffusion in austenite. Numerical simulations of ledgewise growth[70,71] support this assumption that when the ratio of the interledge spacing to the ledge height is relatively small, the reaction times are long and the supersaturation is relatively high. The growth kinetics can then be modeled in the usual manner, with a flux balance equation for the C component.

The migration of the $\alpha:\gamma$ boundary is envisioned to involve several steps. In the first, the substitutional solute concentration in the moving $\alpha:\gamma$ boundary adjusts from the concentration present during nucleation to a value dependent upon the growth kinetics. This latter concentration is a function of chemical and elastic interactions between solute atoms and the boundary. The transient period during which the substitutional concentration in the boundary is acquired is expected to be short. Since substitutional species are highly mobile within the boundary,* they can be "swept up" by the advancing boundary.[47] The volume of the boundary is small relative to the volume of the ferrite, so a change in the boundary concentration will produce a negligible change in the ferrite composition. For this reason, the concentration of X in the boundary is permitted to vary independently of the bulk concentration.

*The boundary diffusivity of substitutional solutes in iron is roughly of the same magnitude as the carbon diffusivity in austenite.[95]

Once the steady-state concentration of X in the boundary is attained, the carbon concentrations in ferrite and in austenite in contact with the boundary are determined by a constrained, local type of equilibrium among ferrite, the ferrite:austenite boundary, and austenite. The Gibbs free energy of the system is minimized subject to the condition that exchange of substitutional atoms among the three phases does not occur (once the kinetic boundary composition has been established). This can be alternately stated as the equilibration of carbon chemical potentials among these phases, but based upon what amounts to, at our present level of understanding, an essentially arbitrary potential in the mobile areas of ferrite:austenite boundaries. The procedure is similar to the familiar paraequilibrium concept[48,96] but now with the addition of a boundary phase between ferrite and austenite.

The departure of the present approach from bulk paraequilibrium (*i.e.*, paraequilibrium between the ferrite and austenite without explicit consideration of the intervening interphase boundary) is that the composition of the $\alpha:\gamma$ boundary "phase" is allowed to depend upon kinetic factors rather than upon local thermodynamic equilibrium. Because the $\alpha:\gamma$ boundary does not reach full equilibrium with the adjacent bulk phases, the Gibbs (or some other) adsorption isotherm is not utilized to determine the boundary composition. Instead, though not considered explicitly, solute concentrations in the $\alpha:\gamma$ boundary are permitted to depend on factors such as the boundary structure and velocity; thus, the ratio of substitutional solute atoms to iron atoms in the $\alpha:\gamma$ boundary may differ from this ratio in the bulk phases.

Because the X and C concentrations in the boundary cannot presently be calculated *a priori*, they will first be treated parametrically. In addition, the adjustments in the boundary composition are taken to occur rapidly compared to the equilibration of carbon chemical potentials in ferrite and austenite, since the latter require long-range volume diffusion of carbon. This last assumption amounts to a quasi-static approach to the problem. The time dependence of the growth kinetics, however, is retained in the conventional growth equation. On this approach, the SDLE on growth is exerted through an adjustment to the boundary conditions of this equation.

Following earlier proposals,[14,19,47] it is suggested that the $\alpha:\gamma$ boundary composition during growth determines the operative C chemical potential in the ferrite and especially in the austenite in contact with this boundary.

Since the bulk phases must communicate through the boundary region, it is reasonable to postulate that the carbon concentrations in the bulk phases are determined by a constrained* equilibrium with the boundary phase.

*This is defined as no exchange of substitutional atoms between any two phases once the boundary composition has been established.

For a given $\alpha:\gamma$ boundary composition (which is determined by kinetic factors), the concentrations of C in ferrite and in austenite in contact with the boundary are determined by the condition that the chemical potential of carbon in the bulk phases at the boundary is the same as the carbon potential within the boundary.

There is an important distinction between the proposed SDLE and the more familiar impurity or solute-drag models applied to grain growth[63–66] or to massive transformations.[97] According to these models, grain boundary concentrations are also a function of velocity, but the boundary velocity is related to a drag force which results from the binding of solute atoms to the boundary or to a dissipation of free energy arising from diffusion across the boundary. The drag force described here results from a change in C partitioning due to nonequilibrium concentrations of carbon and of substantial solute in the $\alpha:\gamma$ boundary. Although the boundary composition may be related to the binding energy of the solutes to the boundary or to a cross-boundary diffusivity, this information is not required to determine the drag force, and unlike the previous solute-drag models, the boundary velocity on the present approach is not considered explicitly and need not be constant.

To determine the magnitude of the SDLE exerted by a specific alloying element upon the growth kinetics of ferrite, one must know the activity of C in the ferrite:austenite boundary during growth. Strictly speaking, the thermodynamic description of the boundary phase depends upon the properties of the bulk phases and the interfacial free energy. However, the proper Gibbsian description of the boundary is difficult to apply in this case due to the lack of information on solute adsorption at $\alpha:\gamma$ boundaries in Fe-C-X alloys. Alternatively, the activity of C in the $\alpha:\gamma$ boundary may be estimated from an equilibrium boundary composition and assumed activity functions. The following procedure was accordingly employed to estimate the required information. Chemical potential functions were obtained from the Hillert-Staffansson model.[98] The solution constants for ferrite:austenite boundaries in Fe-C-Mo were fitted to an *equilibrium* boundary composition estimated from experimentally determined equilibrium austenite grain boundary,[69] ferrite grain boundary,[68] and ferrite:austenite boundary compositions,[58] extrapolated to down to 585 °C, the temperature at which FIM/AP data were secured on the $\alpha:\gamma$ boundary composition[94] in an Fe-0.19 wt pct C-1.81 wt pct alloy. The equilibrium C and Mo concentrations in $\alpha:\gamma$ boundaries were estimated to be 15 at. pct C and 20 at. pct Mo in this alloy at 585 °C. The C and Mo concentrations in the $\alpha:\gamma$ boundary during growth were then varied parametrically, and the concentrations of C in bulk ferrite and in bulk austenite in contact with the $\alpha:\gamma$ boundary were computed by equating the chemical potential of C, μ_C, in ferrite and in austenite with its value in the $\alpha:\gamma$ boundary; *i.e.*, $\mu_C^\alpha = \mu_C^\phi$ and $\mu_C^\gamma = \mu_C^\phi$, where ϕ denotes the $\alpha:\gamma$ "boundary phase."

The results of this calculation are presented in Figure 22 by showing X_C^γ, the mole fraction of C in austenite at the $\alpha:\gamma$ boundary, as a function of the mole fractions of C and Mo in the boundary, X_C^ϕ and X_{Mo}^ϕ, respectively. The greater the value of X_C^γ for a given alloy, the higher the C gradient in austenite, the larger the C flux, and thus, the greater the ferrite growth kinetics. Although X_C^γ varies continuously with X_C^ϕ and X_{Mo}^ϕ, it is truncated in Figure 22 at the conventional bulk paraequilibrium value to display more clearly the range of boundary concentrations which yield slower than paraequilibrium kinetics.

The boundary compositions which yield values of X_C^γ less than the paraequilibrium value forecast slower growth kinetics than predicted under bulk paraequilibrium. These conditions are met for a wide range of boundary compositions, especially at lower C and higher Mo concentrations in the boundary. When X_C^γ is depressed to the bulk atom fraction of C in the alloy, 0.0088 in this case, the C gradient in austenite driving growth will be zero, and ferrite growth will cease. Thus, for the particular choice of boundary thermodynamic parameters employed here, the proposed model for the SDLE can produce growth stasis for many combinations of X_C^ϕ and X_{Mo}^ϕ. It is of special interest to note that this model does not require Mo adsorption to the $\alpha:\gamma$ boundary, but only that the combination of the C concentration and the Mo concentration in the boundary produces a lower value of the carbon activity in the boundary than that determined from bulk paraequilibrium.

The compositions of $\alpha:\gamma$ interfaces formed in Fe-0.19 wt pct C-1.81 wt pct Mo at 585 °C for 30 seconds has been measured recently with an FIM/AP[94] and permit a test to be made of this SDLE model. From the transformation curve for this alloy and temperature (Figure 13(h)), it is evident that the reaction time of 30 seconds is within the first transformation stage, *i.e.*, before transformation stasis has developed. As has been discussed in some detail, the SDLE should be operative under these conditions. The measured $\alpha:\gamma$ boundary

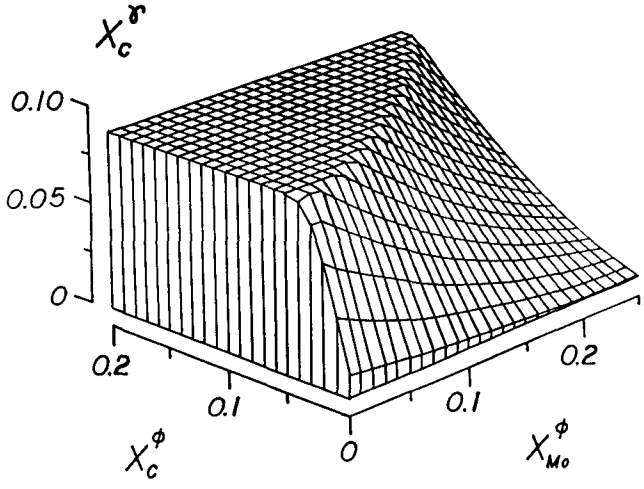

Fig. 22—The calculated mole fraction of carbon in austenite at the $\alpha:\gamma$ boundary, X_C^γ, as a function of the carbon and molybdenum concentrations within the $\alpha:\gamma$ boundary. Fe-0.19 wt pct C-1.81 wt pct Mo, reacted at 585 °C; at paraequilibrium, $X_C^\gamma = 0.09$.

concentrations are $X_C^\phi = 0.08$ and $X_{Mo}^\phi = 0.027$.[94] From Figure 22, slow ferrite growth is not expected since X_C^γ is greater than the paraequilibrium value; *i.e.*, the calculated value is above the truncated plateau. However, it is probable that the measured value of X_C^ϕ is *not* the value that was present during growth. Because of the high diffusivity of C in both austenite and in ferrite and the difficulty of quenching-in the value of X_C^ϕ present at 585 °C,[94] the measured X_C^ϕ should actually be that characteristic of a considerably lower reaction temperature. The temperature below which the C concentration in $\alpha:\gamma$ boundaries can be retained with the experimental conditions employed has been estimated to lie between 450 °C and 370 °C.[94] Thus, the value of X_C^ϕ actually present during growth at 585 °C was almost certainly less than 0.08. As a crude estimate, if the boundary condition is assumed to scale with the paraequilibrium Ae3, the value of X_C^ϕ at 585 °C would be approximately 0.04, roughly half the value of X_C^ϕ at 370 °C. From Figure 22, this X_C^ϕ results in a value of X_C^γ of approximately 0.087 (the paraequilibrium X_C^γ at 585 °C is 0.090), corresponding, in turn, to a parabolic rate constant of 2.3 $\mu m/s^{1/2}$, an 8 pct reduction from the paraequilibrium value of 2.5 $\mu m/s^{1/2}$. Although this reduction in the growth constant is not large, it does demonstrate that the present approach can produce slower ferrite growth than predicted under paraequilibrium conditions. To achieve growth stasis, X_C^γ must be reduced to the bulk carbon concentration, 0.0088. This requires significantly more Mo or less C within the $\alpha:\gamma$ boundary than was reported. Two factors appear to bear primary responsibility for this discrepancy. First, the measured boundary concentrations of C and of Mo are averaged over a randomly chosen area of the $\alpha:\gamma$ boundary. These values may not accurately reflect the compositions in the widely separated[99] mobile portions of the $\alpha:\gamma$ boundary responsible for growth. The uncertainty in the measured X_C^ϕ is carried through calculation of the parabolic rate constant. Second, the solution parameters for the $\alpha:\gamma$ boundary are unknown. Without this information, the shape of the surface in Figure 22 and the magnitude of the SDLE cannot be accurately established. The calculations reported here are thus intended primarily to present an approach to quantifying the SDLE rather than to offer a quantitatively meaningful calculation of the strength of this effect at a given reaction temperature and time in a particular alloy.

D. *On Identifying Bainite in Fe-C-Mo Alloys*

There is still considerable debate in the literature as to what should properly be called bainite. The three definitions in common usage, the surface relief,[27] the overall reaction kinetics,[2,13,15] and the generalized microstructural[14] definitions have been shown to refer to different transformation phenomena.[14,100] The results of this investigation and of a previous study on Fe-C-Mo alloys[1] clearly illustrate some of the contradictions among the three definitions.

On the surface relief definition, bainite consists of ferrite plates which exhibit an invariant plane strain relief effect at a free surface.[27] In the higher Mo-containing Fe-C-Mo alloys employed in the present study, ferrite plates are not observed at temperatures between T_b and slightly below the upper nose in the TTT curve for initiation of transformation.[1,19] The degenerate Widmanstätten structure formed below T_b does not produce an invariant plane strain relief on the scale of optical microscopy (Figure 4(a)). Thus, surface relief bainite is not present in the temperature-composition region investigated.

On the overall reaction kinetics view, bainite forms in the temperature range of the lower "C" curve on the TTT diagram. The product should also exhibit the incomplete transformation phenomenon just below the B_s (*i.e.*, below T_b). However, in Fe-C-Mo alloys, the presence of transformation stasis is composition-dependent (Figure 17); it is not a general characteristic of transformation below T_b. In addition, the T_0 temperature, the upper limit of bainite formation by a martensitic mechanism, is usually in poor agreement with the bay temperature in Fe-C-Mo alloys.[14] For example, in Fe-0.19 wt pct C-1.81 wt pct Mo, T_0 is 750 °C (calculated using the Hillert-Staffansson model[50]), and the bay temperature is 615 °C.

The interpretation of the shape of the TTT diagram in terms of bainite and pearlite "C" curves[13] is clearly inaccurate in Fe-C-Mo alloys and probably in other alloy steels as well. As previously indicated, pearlite formation becomes increasingly rare with increasing Mo concentration.[23] In the Fe-0.19 wt pct C-1.81 wt pct Mo alloy, there is a negligible amount of pearlite formation despite the presence of well-defined upper and lower "C" curves (Figure 1). The upper "C" curve in this alloy results from ferrite and alloy carbide precipitation in a variety of nonpearlite morphologies. Thus, the criteria of the overall reaction kinetics definition of bainite do not apply at all well to Fe-C-Mo alloys.

Microstructural bainite is defined as any nonlamellar, noncooperative, eutectoid decomposition product.[14] This includes ferrite + interphase boundary carbide mixtures formed above and below T_b. Because transformation stasis occurs before carbide precipitation, the incomplete reaction phenomenon is considered to be associated with the proeutectoid ferrite reaction and not with microstructural bainite. Bainite is not confined to temperatures below T_b but can form at temperatures up to the relevant eutectoid temperature range. The advantages of this definition are its lack of ambiguity and its general applicability. It relies upon the structure of the reaction product for identification. The surface relief and overall reaction kinetics definitions identify bainite in terms of features of a presumed martensitic reaction mechanism. Aside from the objections which have been raised as to the viability of a displacive mechanism for the bainite reaction,[14,100,101] these two definitions should be discarded because they either fail to discriminate reliably between reaction mechanisms (surface reliefs) or they depend upon phenomena which are caused by special alloying elements and are insufficiently general (*i.e.*, incomplete transformation).

V. SUMMARY

The overall kinetics of isothermal transformation of austenite to bainite were studied with quantitative optical

metallography and TEM in a series of high-purity Fe-C-Mo alloys containing from 0.06 to 0.27 wt pct C and from 0.23 to 4.28 wt pct Mo at reaction temperatures mainly below that of the bay in the TTT curve for initiation of transformation. Limited studies were also made of the thickening kinetics of grain boundary allotriomorphs below T_b. The results and conclusions are summarized as follows:

1. Occurrence of the incomplete transformation phenomenon, or transformation stasis, depends upon the C and Mo concentrations in Fe-C-Mo alloys. It is not observed in low-C or in low-Mo, Fe-C-Mo alloys. Therefore, it is not a general feature of the bainite reaction.
2. Acceleration of transformation at temperatures below the bay results from the onset of sympathetic nucleation and an increased average growth rate of ferrite. The repeated nucleation of new ferrite crystals causes a repeated reentry into the initial stages of growth, wherein the SDLE is still developing. This permits relatively high (but still diffusion-limited) rates of growth to be achieved.
3. Transformation stasis in Fe-C-Mo alloys can be explained by considering the influence of Mo upon the formation of ferrite. Transformation stasis occurs when the sympathetic nucleation of *carbide-free* ferrite ceases due to carbon enrichment of the remaining austenite. The growth of the first formed ferrite crystals and of the individual sympathetically nucleated ferrite crystals subsequently appearing is restricted by an SDLE. Ferrite and carbide mixtures (*e.g.*, upper and lower microstructural bainite) are not expected to exhibit transformation stasis.
4. Resumption of transformation following transformation stasis is initiated by the precipitation of Mo_2C carbides at $\alpha:\gamma$ boundaries.
5. Ferrite growth kinetics up to 20 °C below T_b in an Fe-0.24 wt pct C-0.93 wt pct Mo alloy do not obey a simple time law. The time exponent itself varies with time and is reminiscent of behavior previously reported for ferrite growth in Fe-C-Mo alloys at temperatures above the bay.[1]
6. The degenerate ferrite morphology formed at temperatures below T_b results from extensive sympathetic nucleation of ferrite and from the restrictions on ferrite growth imposed by the SDLE.
7. The degenerate morphology produces a surface rumpling type of relief; an invariant plane strain surface relief, at least on the scale of optical microscopy, was not found.
8. The absence of the Widmanstätten ferrite morphology, at reaction temperatures between the upper nose and the bay in the TTT curve for initiation of transformation, is due to a reduction in the anisotropy of growth caused by the SDLE and the precipitation of interphase boundary carbides.
9. An approach to calculating the magnitude of the SDLE on ferrite growth is proposed. The C concentrations in ferrite and the C concentration in austenite (both of which govern ferrite growth kinetics) are determined by setting the chemical potentials of C in these phases equal to the chemical potential of C in the boundary. This latter value depends upon the C and the Mo concentrations within the boundary, which, in turn, are set by the boundary migration kinetics rather than by thermodynamic equilibrium. At present, these boundary concentrations must be determined experimentally, *e.g.*, by FIM/AP analysis.

ACKNOWLEDGMENTS

The authors would like to thank the Army Research Office, the Metallurgical Engineering and Materials Science Department of Carnegie Mellon University, Pittsburgh, PA, the American Iron and Steel Institute, Warrendale, PA, the Electric Power Research Institute, Palo Alto, CA, the Office of Naval Research, the National Science Foundation, and the Air Force Office of Scientific Research for supporting this research. The authors would also like to acknowledge Dr. George Spanos (formerly at CMU, now with the Naval Research Laboratory) for many useful discussions.

REFERENCES

1. G.J. Shiflet and H.I. Aaronson: *Metall. Trans. A*, 1990, vol. 21A, pp. 1413-32.
2. F. Wever and H. Lange: *Mitt. Kaiser-Wilhelm-Inst. Eisenforsch.*, 1932, vol. 14, pp. 71-83.
3. F. Wever and W. Jellinghaus: *Mitt. Kaiser-Wilhelm-Inst. Eisenforsch.*, 1932, vol. 14, pp. 105-18.
4. F. Wever and K. Mathieu: *Mitt. Kaiser-Wilhelm-Inst. Eisenforsch.*, 1940, vol. 22, pp. 9-18.
5. H.J. Wiester: *Arch. Eisenhuettenwes.*, 1944, vol. 18, pp. 97-112.
6. H. Lange and K. Mathieu: *Mitt. Kaiser-Wilhelm-Inst. Eisenforsch.*, 1938, vol. 20, pp. 125-34.
7. H. Dopfer and H.J. Wiester: *Arch. Eisenhuettenwes.*, 1935, vol. 8, p. 541.
8. A. Rose and W. Fischer: *Mitt. Kaiser-Wilhelm-Inst. Eisenforsch.*, 1939, vol. 21, p. 133.
9. N.P. Allen, L.B. Pfeil, and W.T. Griffiths: *2nd Report of the Alloy Steels Research Committee*, The Iron and Steel Institute, London, 1939, pp. 369-90.
10. E.P. Klier and T. Lyman: *Trans. AIME*, 1944, vol. 158, pp. 394-419.
11. T. Lyman and A.R. Troiano: *Trans. ASM*, 1946, vol. 37, pp. 402-48.
12. H.A. Smith: *Trans. AIME*, 1935, vol. 116, pp. 342-62.
13. R.F. Hehemann and A.R. Troiano: *Met. Prog.*, 1956, vol. 70, pp. 97-104.
14. H.I. Aaronson: *The Mechanism of Phase Transformations in Crystalline Solids*, Institute of Metals, London, 1969, pp. 270-81.
15. W.T. Griffiths, L.B. Pfeil, and N.P. Allen: *2nd Report of the Alloy Steels Research Committee*, The Iron and Steel Institute, London, 1939, pp. 343-67.
16. A.R. Troiano: *Trans. ASM*, 1949, vol. 41, pp. 1093-1107.
17. J.P. Sheehan, C.A. Julien, and A.R. Troiano: *Trans. ASM*, 1949, vol. 41, p. 1165.
18. M. Hillert: *The Mechanism of Phase Transformations in Crystalline Solids*, Institute of Metals, London, 1969, pp. 231-47.
19. P.G. Boswell, K.R. Kinsman, G.J. Shiflet, and H.I. Aaronson: in *Mechanical Properties and Phase Transformations in Engineering Materials*, S.D. Antolovich, R.O. Ritchie, and W.W. Gerberich, eds., TMS-AIME, Warrendale, PA, 1986, pp. 445-66.
20. M. Enomoto and H.I. Aaronson: *Metall. Trans. A*, 1986, vol. 17A, pp. 1385-97.
21. K.R. Kinsman and H.I. Aaronson: *Transformation and*

Hardenability in Steels, Climax Molybdenum Co., Ann Arbor, MI, 1967, pp. 39-53.
22. H.I. Aaronson, C. Laird, and K.R. Kinsman: *Phase Transformations*, ASM, Metals Park, OH, 1970, pp. 313-96.
23. F.G. Berry and R.W.K. Honeycombe: *Metall. Trans.*, 1970, vol. 1, pp. 3279-86.
24. H. Tsubakino and H.I. Aaronson: *Metall. Trans. A*, 1987, vol. 18A, pp. 2047-60.
25. W.T. Reynolds, Jr., F.Z. Li, C.K. Shui, G.J. Shiflet, and H.I. Aaronson: *Phase Transformations, '87*, G. Lorimer, ed., Institute of Metals, London, 1988, pp. 330-33.
26. W.T. Reynolds, Jr., S.K. Liu, F.Z. Li, S. Hartfield, and H.I. Aaronson: *Metall. Trans. A*, 1990, vol. 21A, pp. 1479-91.
27. T. Ko and S.A. Cottrell: *J. Iron Steel Inst.*, 1952, vol. 172, pp. 307-13.
28. R.F. Hehemann: *Phase Transformations*, ASM, Metals Park, OH, 1970, pp. 397-432.
29. H.M. Clark and C.M. Wayman: *Phase Transformations*, ASM, Metals Park, OH, 1970, pp. 59-114.
30. J.R. Bradley, T. Abe, and H.I. Aaronson: *Rev. Sci. Instrum.*, 1982, vol. 53, pp. 98-99.
31. T. Gladman and J.H. Woodhead: *J. Iron Steel Inst.*, 1960, vol. 194, pp. 189-93.
32. J.E. Hilliard and J.W. Cahn: *Trans. AIME*, 1961, vol. 221, pp. 344-52.
33. C.K. Shui, W.T. Reynolds, Jr., G.J. Shiflet, and H.I. Aaronson: *Metallography*, 1988, vol. 21, pp. 91-102.
34. J.R. Bradley, J.M. Rigsbee, and H.I. Aaronson: *Metall. Trans. A*, 1977, vol. 8A, pp. 323-33.
35. Y. Ohmori: *Trans. Iron Steel Inst. Jpn.*, 1972, vol. 12, pp. 350-57.
36. J.M. Oblak and R.F. Hehemann: *Transformation and Hardenability in Steels*, Climax Molybdenum Co., Ann Arbor, MI, 1967, pp. 15-30.
37. H.I. Aaronson: in *The Decomposition of Austenite by Diffusional Processes*, V.F. Zackay and H.I. Aaronson, eds., Interscience, New York, NY, 1962, pp. 387-546.
38. K.R. Kinsman and H.I. Aaronson: *Transformation and Hardenability in Steels*, Climax Molybdenum Co., Ann Arbor, MI, 1967, pp. 33-38.
39. H.I. Aaronson and C. Wells: *Trans. AIME*, 1956, vol. 206, pp. 1216-23.
40. E.S.K. Menon and H.I. Aaronson: *Acta Metall.*, 1987, vol. 35, pp. 549-63.
41. R.F. Hehemann, K.R. Kinsman, and H.I. Aaronson: *Metall. Trans.*, 1972, vol. 3, pp. 1077-94.
42. G. Spanos and H.I. Aaronson: *Scripta Metall.*, 1988, vol. 22, pp. 1537-42.
43. H.J. Lee, G. Spanos, G.J. Shiflet, and H.I. Aaronson: *Acta Metall.*, 1988, vol. 36, pp. 1129-40.
44. W.T. Reynolds, Jr., S.S. Brenner, and H.I. Aaronson: Carnegie Mellon University, unpublished research, 1987.
45. C. Dube: Ph.D. Thesis, Carnegie Institute of Technology, Pittsburgh, PA, 1948.
46. C. Zener: *J. Appl. Phys.*, 1949, vol. 20, pp. 950-53.
47. J.R. Bradley and H.I. Aaronson: *Metall. Trans. A*, 1981, vol. 12A, pp. 1729-41.
48. M. Hillert: *Jernkontorets Ann.*, 1952, vol. 136, pp. 25-37.
49. J.B. Gilmour, G.R. Purdy, and J.S. Kirkaldy: *Metall. Trans.*, 1972, vol. 3, pp. 1455-64.
50. M. Hillert and L.I. Staffansson: *Acta Chem. Scand.*, 1970, vol. 24, pp. 3618-26.
51. B. Uhrenius: in *Hardenability Concepts with Applications to Steel*, D.V. Doane and J.S. Kirkaldy, eds., TMS-AIME, Warrendale, PA, 1978, pp. 28-81.
52. R. Trivedi and G.M. Pound: *J. Appl. Phys.*, 1967, vol. 38, pp. 3569-76.
53. L. Kaufman, S.V. Radcliffe, and M. Cohen: in *The Decomposition of Austenite by Diffusional Processes*, V.F. Zackay and H.I. Aaronson, eds., Interscience, New York, NY, 1962, pp. 313-52.
54. C. Zener: *Trans. AIME*, 1946, vol. 167, pp. 513-34.
55. H.I. Aaronson and H.A. Domian: *Trans. AIME*, 1966, vol. 236, pp. 781-96.
56. R.F. Hehemann and A.R. Troiano: *Trans. AIME*, 1954, vol. 200, pp. 1272-80.
57. K.C. Russell: *Metall. Trans.*, 1971, vol. 2, pp. 5-12.
58. I. Stark and G.D.W. Smith: in *Phase Transformations '87*, G. Lorimer, ed., Institute of Metals, London, 1988, pp. 475-81.
59. C. Zener: *Trans. AIME*, 1946, vol. 167, pp. 550-95.
60. J.M. Rigsbee and H.I. Aaronson: *Acta Metall.*, 1979, vol. 27, pp. 365-76.
61. C. Li, V. Perovic, and G.R. Purdy: in *Phase Transformations '87*, G. Lorimer, ed., Institute of Metals, London, 1988, pp. 326-29.
62. G.R. Purdy: *Scripta Metall.*, 1987, vol. 21, pp. 1035-38.
63. K. Lucke and K. Detert: *Acta Metall.*, 1957, vol. 5, pp. 628-37.
64. J.W. Cahn: *Acta Metall.*, 1962, vol. 10, pp. 789-98.
65. K. Lucke and H.P Stuwe: in *Recovery and Recrystallization of Metals*, L. Himmel, ed., Interscience, New York, NY, 1963, p. 171.
66. K. Lucke and H.P. Stuwe: *Acta Metall.*, 1971, vol. 19, pp. 1087-99.
67. M. Hillert and B. Sundman: *Acta Metall.*, 1976, vol. 24, pp. 731-43.
68. Ph. Domoulin, M. Guttmann, M. Foucault, M. Palmier, M. Wayman, and M. Biscondi: *Met. Sci.*, 1980, vol. 14, pp. 1-15.
69. M. Enomoto, C.L. White, and H.I. Aaronson: *Metall. Trans. A*, 1988, vol. 19A, pp. 1807-18.
70. M. Enomoto: *Acta Metall.*, 1987, vol. 35, pp. 935-45.
71. M. Enomoto: *Acta Metall.*, 1987, vol. 35, pp. 947-56.
72. H.I. Aaronson, M.R. Plichta, G.W. Franti, and K.C. Russell: *Metall. Trans. A*, 1978, vol. 9A, pp. 363-71.
73. T. Obara, G.J. Shiflet, and H.I. Aaronson: *Metall. Trans. A*, 1983, vol. 14A, pp. 1159-67.
74. S.K. Liu, W.T. Reynolds, Jr., H. Hu, G.J. Shiflet, and H.I. Aaronson: *Metall. Trans. A*, 1985, vol. 16A, pp. 457-66.
75. G.R. Speich and M. Cohen: *Trans. AIME*, 1960, vol. 218, pp. 1050-59.
76. G.R. Speich: in *The Decomposition of Austenite by Diffusional Processes*, V.F. Zackay and H.I. Aaronson, eds., Interscience, New York, NY, 1962, pp. 353-67.
77. M. Hillert: unpublished research quoted in L. Kaufman, S.V. Radcliffe, and M. Cohen: *The Decomposition of Austenite by Diffusional Processes*, V.F. Zackay and H.I. Aaronson, eds., Interscience, New York, NY, 1962, pp. 313-352.
78. R.H. Goodenow, S.J. Matas, and R.F. Hehemann: *Trans. AIME*, 1963, vol. 227, pp. 651-57.
79. M.M. Rao and P.G. Winchell: *Trans. AIME*, 1967, vol. 239, pp. 956-60.
80. R.D. Townsend and J.S. Kirkaldy: *Trans. ASM*, 1968, vol. 61, pp. 605-19.
81. E.P. Simonen, H.I. Aaronson, and R. Trevedi: *Metall. Trans.*, 1973, vol. 4, pp. 1239-45.
82. C. Laird and H.I. Aaronson: *Acta Metall.*, 1967, vol. 15, pp. 73-103.
83. C. Laird and H.I. Aaronson: *Trans. AIME*, 1968, vol. 242, pp. 591-96.
84. W.T. Reynolds, Jr. and H.I. Aaronson: *Scripta Metall.*, 1985, vol. 19, pp. 1171-76.
85. T. Furuhara and H.I. Aaronson: *Scripta Metall.*, 1988, vol. 22, pp. 1509-14.
86. A. Hultgren: *Trans. ASM*, 1947, vol. 39, pp. 915-89.
87. R.C. Sharma and G.R. Purdy: *Metall. Trans.*, 1973, vol. 4, pp. 2303-11.
88. G.R. Purdy: *Acta Metall.*, 1978, vol. 26, pp. 487-98.
89. C.J. Middleton and D.V. Edmonds: *Metallography*, 1977, vol. 10, pp. 55-87.
90. M. Enomoto: *J. Appl. Phys.*, 1980, vol. 51, pp. 818-19.
91. H.I. Aaronson: *J. Microscopy*, 1974, vol. 102, pp. 275-300.
92. H.J. Lee and H.I. Aaronson: *J. Mater. Sci.*, 1988, vol. 23, pp. 150-60.
93. C.A. Dube, H.I. Aaronson, and R.F. Mehl: *Rev. Met.*, 1958, vol. 55, p. 201.
94. W.T. Reynolds, Jr., S.S. Brenner, and H.I. Aaronson: *Scripta Metall.*, 1988, vol. 22, pp. 1343-48.
95. J. Fridberg, L.E. Torndahl, and M. Hillert: *Jernkontorets Ann.*, 1969, vol. 153, pp. 263-76.
96. A. Hultgren: *Jernkontorets Ann.*, 1951, vol. 135, pp. 403-83.

97. M. Hillert: *Jernkontorets Ann.*, 1957, vol. 140, pp. 757-89.
98. M. Hillert: in *The Decomposition of Austenite by Diffusional Processes*, V.F. Zackay and H.I. Aaronson, eds., Interscience, New York, NY, 1962, pp. 197-237.
99. K.R. Kinsman, E. Eichen, and H.I. Aaronson: *Metall. Trans. A*, 1975, vol. 6A, pp. 303-17.
100. H.I. Aaronson and H.J. Lee: *Scripta Metall.*, 1987, vol. 21, pp. 1011-16.
101. H.I. Aaronson and W.T. Reynolds, Jr.: in *Phase Transformations '87*, G. Lorimer, ed., Institute of Metals, London, 1988, pp. 301-08.